

Bottom-Up Reconstruction Scenarios for (un)constrained MSSM Parameters at the LHC

J.-L. Kneur and N. Sahoury

Laboratoire de Physique Théorique et Astroparticules, Université Montpellier 2,
UMR5207–CNRS, F–34095 Montpellier Cedex 5, France.

Abstract:

We consider some specific inverse problem or “bottom-up” reconstruction strategies at the LHC for both general and constrained MSSM parameters, starting from a plausibly limited set of sparticle identification and mass measurements, using mainly gluino/squark cascade decays, plus eventually the lightest Higgs boson mass. For the three naturally separated sectors of: gaugino/Higgsino, squark/slepton, and Higgs parameters, we examine different step-by-step algorithms based on rather simple entirely analytical inverted relations between masses and basic MSSM parameters, including also radiative corrections as reasonably good approximations of the more complete available calculations. We distinguish the constraints obtained for a general MSSM from those obtained with universality assumptions in the three different sectors. Our results are compared at different stages with the determination from more standard “top-down” fit of models to data, and finally combined into a global determination of all the relevant parameters. Our approach gives complementary information to more conventional analysis, and is not restricted to the specific LHC measurement properties. In addition, the bottom-up renormalization group evolution of general MSSM parameters, being an important ingredient in this framework, is illustrated as a new publicly available option of the MSSM spectrum calculation code “SuSpect”.

1 Introduction

If supersymmetry shows up at the LHC, it may be that only a limited part of the predicted Minimal Supersymmetric Standard Model (MSSM)[1] sparticles will be discovered and some of their properties measured. Hopefully, the lightest Higgs scalar h could be discovered, and some of the squarks and the gluino could be copiously produced (if not too heavy) at the LHC due to their strong interactions. In addition some of the neutralinos, including the lightest supersymmetric sparticle (LSP), could be identified and have their masses extracted indirectly from detailed study of squark and gluino cascade decays[2, 3, 4]. Beyond that, the discovery and measurement of the full set of MSSM sparticles may be very model dependent and anyway challenging in many scenarios at the LHC. Various analysis have been conducted (see e.g. [5, 6]) to determine the basic MSSM parameter space from the above assumed experimental measurements. A widely illustrated strategy, in a so-called “top-down” approach, is to start from a given supersymmetry-breaking model at very high grand unification scale, predicting for given input parameter values the superpartner spectrum at experimentally accessible energy scales, and next fitting this spectrum (together with possibly other observables like cross-sections etc) to the data in order to extract constraints on the basic model parameters. Constraints from past and present collider and non-collider data, with consequent prospects for the LHC and future linear collider (ILC), have been analyzed typically from systematic scanning of MSSM parameter space[7, 8] (though mostly in the constrained minimal supergravity (mSUGRA) [9] case). In addition, more elaborated χ^2 fitting procedure (or some generalizations[10, 11]) have been also used in many such studies, together with Monte-Carlo or other process simulation tools[12, 13, 14] as well as more specific tools for parameter determination[15, 16]. On general grounds fitting and minimization procedures are efficient when the number of independent measurements is (much) greater than the number of fitted parameters of the underlying model, and provided that data are reasonably accurate. But clearly it becomes less controllable¹ if considering e.g. the most general MSSM[1] with about 22 arbitrary basic parameters even when neglecting flavor mixing in the sfermion sector. Alternatively, so-called inverse or bottom-up reconstruction approaches are often motivated[19, 20, 21, 22, 6, 23, 24]. Also it recently appeared a growing number of analysis for the LHC or the ILC, attempting to go beyond conventional top-down fitting techniques[24] or supplementing these with more elaborated frequentist or Bayesian methods, with Markov chain Monte-Carlo (MCMC) techniques in particular[8, 25, 17]. Yet it has been stressed (for instance in refs. [24]) that the mapping from LHC data to the underlying basic MSSM parameters may be far from being unique. However, most works still essentially rely on simulations tools fed with top-down MSSM Lagrangian-to-spectrum relations, while to our knowledge reconstruction scenarios based on explicitly inverted relations (see e.g. [19, 20, 21, 22]) appear not so widely explored in the literature. Moreover many concrete reconstruction of MSSM parameter studies[16, 5, 6] often considered rather optimistic LHC or ILC scenarios in the sense that results are presented assuming that most, if not all, MSSM sparticles masses and other rele-

¹See however ref.[17] for a recent elaborated treatment of multi-parameter cases with both frequentist and Bayesian approaches, also including Markov Chain Monte-Carlo (MCMC) techniques[18].

vant observables have been measured with the best expected accuracy. At the same time it is often assumed that the more constrained mSUGRA model[9] with four continuous plus one discrete parameters) is to be determined. While such studies are certainly very useful guidelines for LHC and ILC analysis, these assumptions may be considered quite optimistic for the supersymmetry discovery prospects in general, specially at the LHC. It is thus worth to develop alternative (or rather complementary) strategies to foresee more pessimistic scenarios, still trying to extract as much as possible informations on the nature of the underlying supersymmetry-breaking model in case that only a handle of the predicted sparticles would be identified.

In this paper we explore specific bottom-up reconstructions, at first more restricted and certainly far from being fully realistic as concerns data simulation, but that we expect to be useful and complementary to the more standard simulation tools. Our approach is starting from analytical inverse relations between the measured masses and basic parameters. This “inverse mapping” for the MSSM spectrum has been investigated to some extent in the past years[19, 20] but mainly at the tree-level approximation, and moreover much often in the context of the ILC data essentially. It is generally expected that simple analytic expressions between observables and parameters are more transparent or insightful than purely numerical results, providing e.g. explicit correlations among parameters. Particularly in the MSSM, even at tree-level, this connexion is already quite involved so that it is difficult to grasp a good intuition on the sensitivity of the different observables to MSSM parameters unless having spend much time in doing fits and related calculations. But more concretely than a useful insight, we also hope that such an approach could suggest new strategies for reconstruction of parameters, as will be illustrated here. For example, by exploiting well-known relations between the (first two generation) squark and slepton soft mass parameters and physical masses, including the renormalization group evolution (RGE) dependence[26, 27], we construct appropriate combinations of observables in this squark/slepton sector which appear to provide interesting and almost model-independent constraints.

In fact, deriving analytic inversion relations in the MSSM may appear at first a rather academic exercise, quite remote from the complexity of the actual experimental situation especially at the LHC. This is because such inverted mapping remains relatively simple only if restricted to the tree-level approximation, becoming a priori inextricable if including radiative corrections, that are certainly necessary at the accuracy level expected for realistic LHC and ILC data analysis. More precisely through loop contributions almost all sparticle masses have a cumbersome dependence on almost all MSSM parameters. Still, we will see how radiative corrections can be incorporated into our framework rather simply, essentially by (numerical) iterative procedure in a manageable way, in reasonable but often realistic approximations. We emphasize that this procedure is very similar to the way in which radiative corrections are included in more conventional top-down MSSM spectrum calculations[28, 29, 30, 31] and it allows to keep most advantages of the bottom-up approach.

Even if one can incorporate a fair amount of presently know radiative corrections into this framework, we stress that our motivation is not to compete with the state of the art in present analysis of MSSM constraints at LHC, merely by replacing elaborated simulations tools with a bunch of rather simple analytic relations (and simple combinations of data uncertainties as we will

see). Accordingly our analysis is at this stage still essentially a theoretical exercise, not incorporating important ingredients of the complexity of LHC measurements (such as detailed event selections, detector properties etc) that are ultimately necessary and pave the non-trivial steps in going from basic LHC data to sparticle mass measurements. Yet our aim is to consider as much as possible realistic and minimal LHC sparticle identifications, using a limited set of sparticle mass measurements. We then gradually consider different SUSY-discovering scenarios, going from minimal input assumptions to more optimistic ones, defining corresponding algorithms with definite input/output parameters. This step-by-step analysis may turn out to be closer to the actual experimental situation where one will certainly not identify all sparticles at once, even for the most optimistic expectations. Though our analysis essentially concentrates on particles expected to be accessible at the LHC, it will appear that some of the reconstruction algorithms used here could apply more or less directly to ILC measurements upon appropriate changes in data accuracies. We thus make occasionally some comments on ILC prospects, but refrain to enter a detailed ILC analysis which is beyond the scope of the present paper, since other expected sparticle mass measurements at the ILC would need rather different algorithms (though quite similar in spirit).

The paper is organized as follows: in section 2 we briefly define and review a plausible set of sparticle mass measurements at the LHC, with accuracy on which is based our analysis. We consider different levels of assumptions on the nature and number of identified sparticles, defining several scenarios. We also gradually introduce universality assumptions on the different sector soft-SUSY breaking parameters. In sections 3-6 we expand results of analytic inversion analysis, some already presented in ref. [19] for different parameter sectors of the MSSM, recasting those results in the context of gluino/squark cascade decay mass measurements at the LHC, and incorporating radiative corrections. We consider separately four different sector: gaugino/Higgsino parameters (section 3); squarks and sleptons (first and second generation) (section 4); third generation squarks (section 5); and finally the Higgs parameter sector in section 6. These distinctions are quite natural when considering both the interdependence between observables and parameters and the experimental signatures expected at LHC from a given sector. We will delineate which relations and results are valid in a general (unconstrained) or a more constrained MSSM (with universality relations at the GUT scale). We also compare in some detail at different stages our reconstruction results with more standard top-down fitting procedure using MINUIT χ^2 minimization[11], with data and fitted parameters directly set by the above step-by-step scenarios rather than by performing “all at once” global fits. Conclusion and outlook are given in section 7.

Finally we discuss in Appendix the properties of the bottom-up renormalization group evolution, a necessary ingredient in this approach, implemented as an option of the SuSpect code[31]. Important features like the error propagation from low to high energy parameters that is implied by RGE are illustrated there.

2 Bottom-up strategy from plausible LHC measurements

At the LHC, the dominant production of pairs of gluinos or squarks (or gluinos associated with squarks) is expected due to their strong interaction. The corresponding cross-sections are large for moderate masses but decrease rapidly for large gluino and/or squark masses. Prospects of discovery of gluino and squarks with masses up to a few TeVs are reported[32, 33, 5], depending on the luminosity (and depending of course on the details of the supersymmetric models and spectra).

2.1 Mass measurements from gluino/squark cascade decays

From detailed study of gluino/squark cascade decay products at the LHC, masses of the sparticles involved can be determined with quite good accuracy (a few percent) using the so-called kinematic endpoints method[3, 4]. For a typical mSUGRA benchmark point like SPS1a [34] which has been intensively studied in simulations, the masses of the sparticle involved in the gluino and squark decays is obtained from analysis of exclusive chain of (2-body) cascade decays, typically[4]:

$$\tilde{g} \rightarrow \tilde{q}_L(\tilde{b})q(b) \rightarrow \chi_2^0 q_f q \rightarrow \tilde{l}_R l q_f q \rightarrow \chi_1^0 l_f l q_f q . \quad (1)$$

(Note however that we will subsequently use these data as a blind input with the aim to go beyond the SPS1a benchmark (or even beyond a mSUGRA model) as concerns the basic MSSM parameter reconstruction.)

Actually the four masses of \tilde{q}_L , \tilde{e}_R and $\chi_{1,2}^0$ can be determined from the cascade decay starting from the \tilde{q}_L . The gluino mass can then be determined from the decay to \tilde{b} (see B. Gjelsten et al p.213 in [5]). Alternatively in ref. [4] the gluino mass as well as the four other masses are determined from the full cascade Eq. (1). The sparticle mass determinations and accuracies assumed here are based on the results of ref. [4] together with ref. [5], summarized in Table 1. These accuracies in 1 may be subject to some adjustments or updates due to eventually more refined analysis, and should be considered here as illustrative, without drastically changing our procedure and results. (For instance very recently even better prospects on mass accuracies have been reported[35, 36] by exploiting correlated decays of two such cascades.)

Among the different selection criteria, an important characteristic one is to look for two isolated, opposite sign, same flavour e, μ leptons[5, 4]. We will not be involved however here with a concrete analysis of these cascade events, and rather use directly the expected mass measurements extracted from such studies. We refer to these references for more details and shall here only briefly mention some of their main features. For typical benchmark points like SPS1a or other cases[34] more sparticles than those present in Eq. (1) are in principle accessible, from independent processes. (Indeed the slepton \tilde{l}_R is also measured independently of the cascade (1) from slepton pair production). Some of the other sparticles may be more difficult to identify, due e.g. to the fact that neutralinos, and charginos decay predominantly into $\tilde{\tau}$ and τ , experimentally more challenging to detect than a dilepton signal typically[5]. (These effects are more pronounced for large $\tan \beta$ due to a larger mixing). Though gluinos decay predominantly in \tilde{q}_L squark, and $\tilde{\chi}_2$ predominantly in \tilde{l}_R

slepton, the mass measurements of \tilde{q}_R (and \tilde{l}_L) are also possible[5], but may be less favored by the small $\tilde{g} \rightarrow \tilde{q}_R q$ branching ratio (B.R.) with respect to other channels, though final statistics can be sufficient[5]. Moreover \tilde{q}_R decays directly into $\tilde{\chi}_1$, since $\tilde{\chi}_1$ is mainly Bino for SPS1a (and this is more or less so in most mSUGRA cases as well, similarly $\tilde{\chi}_2$ is essentially Wino). Thus, \tilde{q}_R being $SU(2)$ singlet, it decays into the corresponding q_R quark together with $\tilde{\chi}_1$ with a B.R. of almost 100%.

Table 1: different plausible gradually optimistic assumptions on the amount of sparticle mass measurements at the LHC, from gluino cascade decays and other decays, defining our successive reconstruction scenarios. The corresponding experimental errors on mass determinations quoted here are taken from refs.[2] and [5].

Input scenarios (+theory assumptions)	measured mass	expected LHC accuracy (GeV)	decay or process
(minimal):	$m_{\tilde{g}}$,	7.2	\tilde{g} cascade decay
S_1 (MSSM),	$m_{\tilde{\chi}_1^0}$,	3.7	” ”
S_2 (universality)	$m_{\tilde{\chi}_2^0}$,	3.6	” ”
S_4 ,	$m_{\tilde{q}_L}$,	3.7	” ”
S'_4 (universality)	$m_{\tilde{l}_R}$	6.0	” ”
$S_3 = S_1$ plus:	$m_{\tilde{\chi}_4^0}$	5.1	$\tilde{q}_L \rightarrow \tilde{\chi}_4^0 + \dots$ cascade
S_5 ,	$m_{\tilde{b}_1}$,	7.5	\tilde{g} cascade decay
S'_5 (universality)	$m_{\tilde{b}_2}$	7.9	” ”
$S_6 = S_2 + S'_4 + S'_5$ plus:	m_h	0.25 (exp)–2 (th)	$h \rightarrow \gamma\gamma$ (mainly)

More generally the nature of sparticles involved in such cascades or other considered processes strongly depends on MSSM parameters, i.e. the specific masses, branching ratios and other observables, and also on some properties inherent to the MSSM structure. Thus at present it is hard to guess which process may be actually favoured at the LHC. Indeed the parameter space where decay chains such as in Eq. (1) can occur may be considered already quite specific, as it requires (non-LSP) neutralinos heavier than the first two generation sleptons, but light enough to be produced by gluinos and squarks. Accordingly we insist that considering in this work only the sparticle masses accessible from the decay (1) (plus the lightest Higgs) is not a strong prejudice against the possibilities of other processes and extra sparticle identification. As motivated in introduction, it is simply to consider what this approach can do from a well-defined “minimal” input set, and indeed most of our inversion algorithms could be easily extended if more (or different) sparticles will be available.

Another important feature of the decay in Eq. (1) is that there is no way to distinguish the different squarks \tilde{q} from each others: this is not so much a property of this specific decay but rather due to the fact that there is no realistic mean at present of tagging light quark charge and/or flavor (moreover they all have almost indistinguishable B.R.). Accordingly the first squark entering the

decay chain, resulting from the decaying gluino, can be either $\tilde{u}, \tilde{d}, \tilde{c}, \tilde{s}$ or \tilde{b}_1, \tilde{b}_2 (in general it could also be \tilde{t}_1, \tilde{t}_2 but this is not kinematically allowed for the SPS1a input parameters[4, 5]). One can identify the \tilde{b} to some extent: the decay of gluino into \tilde{b}_1 is dominant over the \tilde{b}_2 one due to the smaller mass, and \tilde{b}_1 decay leads to b quark that can be tagged. In addition one may be able to extract a signal even for \tilde{b}_2 (i.e. distinguish it from \tilde{b}_1), but with less statistics (correspondingly larger mass error) and only for the large luminosity 300 fb^{-1} [3]. We will thus consider in addition to our minimal input scenario a next scenario where either \tilde{b}_1 alone or both \tilde{b}_1 and \tilde{b}_2 masses are extracted.

Finally, on top of the sparticle masses measured via the gluino cascade, we will consider in section 6 what additional constraints are obtained within our approach if the lightest Higgs mass is assumed to be measured via its $\gamma\gamma$ decay modes[5], which is mainly responsible of the expected accuracy as quoted in Table 1.

2.2 Outline of bottom-up reconstruction algorithms

According to the previous experimental possibilities, we define in Table 1 successive scenarios to be studied and differing on the amount of sparticle masses measured at the LHC, from S_1 to S_6 : Scenarios S_1 - S_3 may be considered to range from a minimal input scenario to gradually more optimistic ones, while some scenarios differ by model assumptions (general MSSM or universality relations typically).

In our study we shall first generate “data” with central values e.g. for the SPS1a benchmark point, by running the code SuSpect[31] for the (constrained MSSM) input:

$$m_0 = -A_0 = 100 \text{ GeV}, \quad m_{1/2} = 250 \text{ GeV}, \quad \tan \beta(m_Z) = 10, \quad \mu > 0. \quad (2)$$

The resulting spectrum in Table 2 is calculated from the latest version 2.41 of SuSpect for two available options on RGE and sparticle mass radiative corrections, both for illustration and the need of our analysis, as will be developed later on. Note that we use everywhere a value of the top mass $m_{top} = 175 \text{ GeV}$ rather than the latest experimental top mass values: $m_{top} = 172.6 \pm 1.4 \text{ GeV}$ [37], in order to be more consistent with the analysis performed in ref.[3, 4]. We assume that this shift in the central value of the top mass should not affect qualitatively our analysis (although what could be important is the impact of the top mass uncertainties).

We will next use the sparticle masses contributing to the gluino cascade as blind input within different reconstruction scenarios, without assuming at first a constrained MSSM with universality relations. The aim is to examine what can be reconstructed under different gradually constrained assumptions on the MSSM parameters. We emphasize that our construction is not at all limited to the SPS1a mSUGRA benchmark scenario, nor even to mSUGRA. We illustrate the determination uncertainties from the SPS1a sparticle mass error as reference since it is one of the most simulated benchmark in the literature.

Apart from distinguishing different scenarios as indicated in Table 1, most of our study is based on specific bottom-up algorithms depending on the assumed input sparticle masses and output ba-

Table 2: Soft and other basic parameters plus sparticle pole masses (relevant to our study) for SPS1a input (with $m_{top} = 175$ GeV) with latest SuSpect ver 2.41, for two illustrative optional choices: 1) full two-loop in RGE and full radiative corrections to sparticle masses (second and fifth columns); 2) one-loop RGE, no radiative corrections to squarks, gluino, neutralinos, charginos masses, simple approximation for m_h radiative corrections (third and sixth columns).

basic par.	2-loop RGE +full R.C.	1-loop RGE +approx. R.C.	relevant pole masses	2-loop RGE +full R.C.	1-loop RGE +approx. R.C.
Q_{EWSB}	465.5	468.2			
M_1	101.5	108.8	$m_{\tilde{N}_1}$	97.2	105.1
M_2	191.6	208.9	$m_{\tilde{N}_2}$	180.8	189.9
M_3	586.6	603.8	$m_{\tilde{g}}$	606.1	603.8
μ	356.9	340.6	$m_{\tilde{N}_4}$	381.8	369.6
$\tan \beta$	9.74	9.75			
$m_{H_d}^2$	$(179.9)^2$	$(187.3)^2$	m_h	110.85	111.28
$m_{H_u}^2$	$-(358.1)^2$	$-(341.7)^2$			
m_{e_L}	195.5	201.5	$m_{\tilde{e}_2}$	142.8	145.4
m_{τ_L}	194.7	200.6			
m_{e_R}	136	138.6			
m_{τ_R}	133.5	136.2			
$m_{Q_L^{1,2}}$	545.8	554.1	$m_{\tilde{u}_1}$	562.3	551.6
$m_{Q_L^3}$	497	502.9	$m_{\tilde{b}_1}$	516.2	502.1
m_{u_R}	527.8	531.6	$m_{\tilde{b}_2}$	546.3	530.1
m_{t_R}	421.5	421.6			
m_{d_R}	525.7	528.7			
m_{b_R}	522.4	525.4			
$-A_t$	494.5	501.0			
$-A_b$	795.2	791.3			
$-A_\tau$	251.7	255.0			
$-A_u$	677.3	686.6			
$-A_d$	859.4	857.2			
$-A_e$	253.4	256.7			

sis parameters. In defining these algorithms it is convenient to consider separately and gradually the three different sectors of gaugino/Higgsino, squark/slepton, and Higgs sector respectively (distinguishing also the third from the first two generations in the squark sector, since those necessitate different treatments due to the mixing in the third generation). We will also carefully distinguish different scenarios depending on the amount of theoretical assumptions, eventually reducing the number of basic MSSM parameters, like universality of gaugino and/or scalar mass terms typically. Our different algorithms obviously depend on specific assumptions, since input and output parameters may be completely different depending on these. We describe in detail in the next sections these particular algorithms depending on the parameter sectors and theoretical assump-

tions considered. The starting points are always tree-level relations giving some basic Lagrangian parameters in terms of appropriate input sparticle masses. For example in the gaugino/higgsino sector we consider typically inverted relations of the generic form

$$f(m_{\tilde{g}}, m_{N_1}, m_{N_2}; \mu, M_1, M_2) + \Delta f_{rad.corr.} = 0, \quad (3)$$

where f gives the output parameters μ, M_1, M_2 in terms of input physical gluino and two neutralino masses: $m_{\tilde{g}}, m_{N_1}, m_{N_2}$, or other similar relations for different input/output choices. Whenever possible, the relations defining f in Eq. (3) are entirely analytical and often giving a linear (unique) or at most quadratic solution (with eventually corresponding twofold solutions). In addition some input/output parameter choices need extra numerical calculations, typically iterations. These are needed anyway to take into account the radiative corrections, symbolized by the term $\Delta f_{rad.corr.}$ in Eq. (3), which generally depends on extra MSSM parameters or masses. As already mentioned, it is clear that such approach cannot be very realistic if not including at least some part of the radiative corrections, as discussed in next subsection.

Once having reconstructed from a relation like (3) the relevant MSSM parameters at the “physical” scale (generally identified as the electroweak symmetry breaking (EWSB) scale), another important step in this bottom-up approach is the possibility of evolving these parameters consistently from low to high (GUT) scale, with implications concerning the propagation of parameter uncertainties from low to high scales. Such bottom-up RGE evolution of soft parameters had been considered in the past [19, 21] (see [21] notably for mass measurement error propagation), but meanwhile many refinements e.g. on radiative corrections have been included in public MSSM codes. Accordingly we have implemented an up-to-date option in the code `SuSpect` to perform this bottom-up RGE, which is used at different stages in our analysis and also illustrated specifically in the Appendix.

2.3 Including radiative corrections in bottom-up reconstruction

We explain here on general grounds how we incorporate radiative corrections into our algorithms, with specific mass/parameter relations to be given later, once having defined algorithms for the different sectors more precisely. Prior to the bottom-up RGE comes the question of incorporating radiative corrections linking the running parameters to the physical (pole) masses, as generically indicated by the terms $\Delta f_{rad.corr.}$ in Eq. (3). Clearly, incorporating the full radiative corrections to *all* sparticle pole masses as given in terms of MSSM parameters, irremediably spoils the possibility of such simple analytic inversions, since complete radiative corrections would introduce, already at one-loop level, highly non-linear dependence upon (almost) all parameters of the MSSM. However, upon assuming a certain level of (reasonably good) approximations for these radiative corrections, it turns out to be relatively easy to incorporate these at a realistic level. This is specially the case for the sparticle masses entering the relevant cascade decays: typically the (first two generation) squarks receive radiative corrections that are largely dominated [38] (at one-loop) by gluon/squark and gluino/quarks QCD corrections, involving precisely the same sparticles enter-

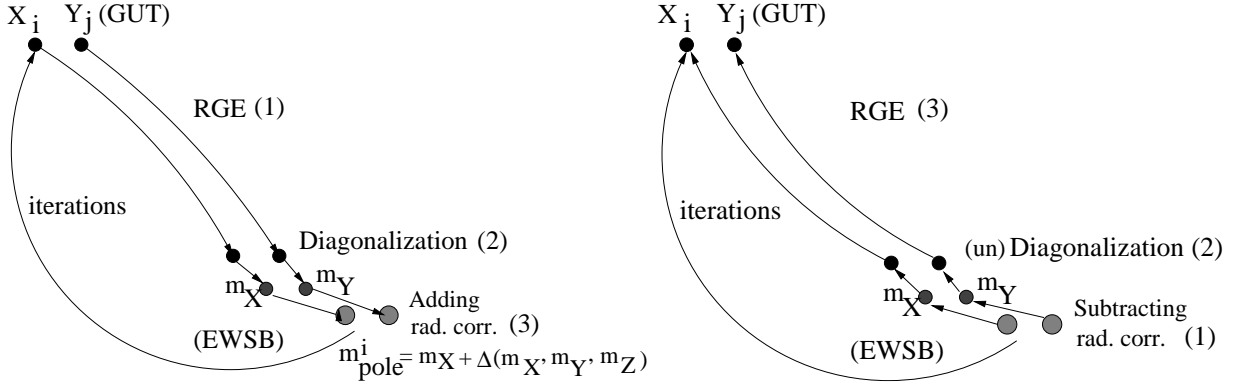


Figure 1: Schematic picture of the top-down (left) and bottom-up (right) mappings and their similarities in practical calculations. X_i and Y_j are a set of (soft or SUSY) running parameters, RG-evolved between GUT and EWSB scales (step 1 or 3 respectively). X_i and Y_j may mix and diagonalization gives (running) mass eigenvalues m_X, m_Y (step 2). Next additional radiative corrections linking running to pole masses m_{pole}^i are added (resp. subtracted) and may depend on extra unknown parameters or masses Z_k, m_k . Iterations are needed at several steps in each approaches, as well as specific assumptions of some a priori unknown parameters.

ing the cascade. Other corrections, like electroweak ones corrections, are fairly negligible[38] in comparison. Similarly, corrections to the gluino mass are essentially dominated by gluon/squark QCD corrections. Consequently it is rather simple to “subtract out” those corrections, starting from the experimentally measured pole masses, and applying next tree-level algorithms to the running masses, eventually applying this procedure in several steps using numerical iterations when needed. Although this procedure may appear rather cumbersome at first, we emphasize that it is very similar to the manipulations that need to be performed in a standard top-down approach, where iterations are anyway necessary in spectrum calculations[31, 29, 30, 28] once including radiative corrections. The similarities between standard top-down and our bottom-up practical calculations are illustrated sketchily in Fig. 1: X_i and Y_j represents some of the relevant (soft or SUSY) running parameters, to be RG-evolved between GUT and EWSB scales (step 1 in the top-down approach or 3 in the bottom-up approach respectively). Then these parameters can have mixing so that diagonalization in step 2 gives (running) mass eigenvalues m_X, m_Y in the top-down case. In the bottom-up case, rather than performing a brute inverted diagonalization, if possible it is more convenient to use at step 2 more appropriate relations among parameters[19] in such a way that the required output MSSM parameters are in one-to-one relations with the accessible input masses. (We will see a specific example of such relations for Eq. 3 in the neutralino sector in section 3 below). Next the necessary radiative corrections linking running to pole masses m_{pole}^i are added (respectively subtracted in the bottom-up case) and these may depend on extra unknown parameters or masses Z_k, m_k (in which case definite assumptions on this unknown parameter space is needed). Iterations are performed in each approaches for the radiative correction steps, since these depend on final sparticle masses. (Iterations are also needed for the RGE since the EWSB

scale and other relevant parameters depend on the sparticle spectrum). In practice the kind of subtractions and other numerical manipulations that are needed specifically here are made easier by a number of possibilities included in the latest version of the SuSpect[31] code². Concerning the neutralino masses, radiative corrections are known to be reasonably small, and moreover to a very good approximation one can incorporate the leading ones in the form of tree-level deviations on the parameter μ , M_1 , M_2 , allowing again subtractions and iteration procedures when applying tree-level reconstruction algorithms. Moreover, once a certain set of MSSM parameters are reconstructed in this way, in some cases we also incorporated the extra unknown radiative corrections by assuming typically universality relations *within* the loop-level calculations. This may induce a little bias, but we consider (and have explicitly checked for the SPS1a case) this to be a reasonably good approximation, even when considering a general MSSM reconstruction.

Concerning the Higgs sector, radiative corrections to the light Higgs mass m_h and pseudoscalar mass m_A are known to be of primary importance. But, as is well known, the leading contributions essentially come from the stop sector, and more generally there are available approximations[39] that are excellent to 1-2 GeV level³, i.e. of the order of higher order uncertainties[40].

On general grounds, even within the present state of the art the known radiative corrections to sparticle and Higgs mass still suffer from uncertainties due to unknown higher orders. Moreover at the LHC experimental errors are generally larger than the latter theoretical errors (except for the lightest Higgs mass m_h). These features evidently affect our analysis, but in the same way as any other more standard top-down approach to the reconstruction of MSSM parameters at the LHC. Clearly the real limitation in incorporating radiative corrections does not come from the eventual complexity of incorporating these numerically within a particular procedure, but rather on the uncertainties resulting from unknown sparticle masses contributing at the loop level to a given observable. In some cases where the latter uncertainties may particularly affect our results, we take these into account as theoretical uncertainties, as will be specified. Overall we consider that our treatment of radiative corrections as described here should be sufficient for our rather limited purpose.

2.4 Treatment of mass uncertainties and interpretation

For the different scenario considered we will illustrate the expected accuracy on the reconstructed parameters for given mass measurement accuracies (eventually considering also theoretical errors). To delineate this error propagation we have performed various scanning over the input mass values within errors, or other relevant MSSM parameters, either with uniformly distributed random numbers or alternatively also using random numbers with a Gaussian distribution (in which case we

²like for example the possibility to “switch off” gradually some of the radiative corrections to the sparticle masses, as illustrated in Table 2.

³The latter approximations are also incorporated as one option in the SuSpect code, alternatively to the full one-loop, or full one-loop plus leading two-loop calculations options.

can define confidence level intervals)⁴. The sparticle mass errors as quoted in Table 1 are however known to be not purely statistical: there is a large part which come from the systematic errors on jet resolution[3, 4], and moreover these errors are also strongly correlated. We stress however that a more involved treatment of uncertainties, properly combining the statistic and systematic ones, taking into account correlations etc, appears quite non-trivial[17] and is beyond the scope of the present paper. One could in principle make substantial improvement in the final determination of parameters by using directly the endpoint measurements[3, 4] of the gluino cascade rather than the naive mass errors obtained from the latter. Consequently, one should keep in mind that the interpretation of the various domains and contours in parameter space that we shall obtain are lacking a very precise statistical significance. (We plan to perform a more refined statistical analysis in the future[41]). Despite these limitations we will illustrate detailed comparisons, for most considered scenarios, of bottom-up determination results with those obtained from more standard statistical treatment with χ^2 minimization in a top-down approach using MINUIT[11].

3 Gaugino/Higgsino parameter determination from gluino cascade

We start by recalling some analytic inversion algorithm at the tree-level, adapted to the input scenarios corresponding to the extractable masses in the gluino decay chain as above discussed. We thus consider the parameters relevant to the gaugino/Higgsino sector. Starting from the neutralino mass matrix:

$$M_N = \begin{pmatrix} M_1 & 0 & -m_Z s_W \cos \beta & m_Z s_W \sin \beta \\ 0 & M_2 & m_Z c_W \cos \beta & -m_Z c_W \sin \beta \\ -m_Z s_W \cos \beta & m_Z c_W \cos \beta & 0 & -\mu \\ m_Z s_W \sin \beta & -m_Z c_W \sin \beta & -\mu & 0 \end{pmatrix} \quad (4)$$

the 4 invariants (under diagonalization transformation):

$$Tr M_N, \quad \frac{(Tr M_N)^2}{2} - \frac{Tr(M_N^2)}{2}, \quad \frac{(Tr M_N)^3}{6} - \frac{Tr M \quad Tr(M_N^2)}{2} + \frac{Tr(M_N^3)}{3}, \quad Det M_N \quad (5)$$

provide a system of equations[19] which can be used in several different ways depending on the choice of input and output parameters. Two equations are actually expressing necessary and sufficient conditions for the existence of solutions to this system (see Appendix B of ref. [19] for more

⁴There are a few cases in our analysis where uniform “flat prior” distributions may give misleading “density” regions for the resulting constraints on some of the parameters (typically for $\tan \beta$, see sec. 4.2 for illustration and discussion). In such cases we made obvious changes for more appropriate non-flat distributions, but have not made any attempt to define much refined priors in a Bayesian approach such as is done notably in [25].

details):

$$P_{ij}^2 + (\mu^2 + m_Z^2 - M_1 M_2 + (M_1 + M_2)S_{ij} - S_{ij}^2)P_{ij} + \mu m_Z^2 (c_W^2 M_1 + s_W^2 M_2) \sin 2\beta - \mu^2 M_1 M_2 = 0 \quad (6)$$

and

$$(M_1 + M_2 - S_{ij})P_{ij}^2 + (\mu^2(M_1 + M_2) + m_Z^2(c_W^2 M_1 + s_W^2 M_2 - \mu \sin 2\beta))P_{ij} + \mu(m_Z^2(c_W^2 M_1 + s_W^2 M_2) \sin 2\beta - \mu M_1 M_2)S_{ij} = 0 \quad (7)$$

where we define for short $S_{ij} \equiv \tilde{M}_{N_i} + \tilde{M}_{N_j}$, $P_{ij} \equiv \tilde{M}_{N_i} \tilde{M}_{N_j}$ where $i, j = 1, \dots, 4$ ⁵, and $s_W = \sin \theta_W$, $c_W = \cos \theta_W$.

Note that Eqs. (6),(7) are originally tree-level relations but, as explained in section 2.3, in our analysis we shall incorporate as much as possible of realistic radiative corrections: to start with, the values of s_W^2 and m_Z in expressions (6),(7) are to be understood as the properly defined \overline{DR} scheme parameters: \bar{s}_W^2 and \bar{m}_Z .

If chargino masses were known at this stage Eqs. (6), (7) would lead rather simply to a unique solution for M_1 for given μ , M_2 and $\tan \beta$ [19], which had been studied in the past e.g. for given chargino and neutralino mass measurement prospects at the ILC. Precise determinations of the chargino/neutralino parameters at the ILC, partly based on analytic (or semi-analytic) inverted relations in the neutralino and chargino sector, have been intensively studied in ref.[20]. Here, since we do not assume chargino masses to be measured in our scenarios, that appear more challenging at LHC anyway, and given the parameters entering the gluino decay of interest here, it is more appropriate to use Eqs. (6), (7) differently as examined in next subsection⁶.

3.1 Scenario S1: determining M_1, M_2 from m_{N_1}, m_{N_2} in non-universal MSSM

Let us first consider a general (unconstrained) MSSM scenario S1 with no universality of gaugino masses assumed, and use Eqs.(6), (7) to determine M_1 and M_2 from the two experimentally measured neutralino masses M_{N_1}, M_{N_2} extracted from the cascade decay, for given μ and $\tan \beta$ parameter input. This gives a unique and relatively simple solution for M_1, M_2 for fixed input parameters: taking central values of the masses M_{N_1}, M_{N_2} plus the reference SPS1a values of μ and $\tan \beta$ we recover the correct SPS1a values of M_1, M_2 . More interesting than this consistency check is to determine the expected accuracy on output parameters, given the experimental uncertainties on neutralino masses, and the presumably limited knowledge on the two other basic parameters μ and $\tan \beta$. This is illustrated in Fig. 2, where domains in the M_1, M_2 plane are shown (as obtained from a scan with (uniformly distributed) random numbers) for accuracies on the two neutralino masses taken from Table 1, and three different assumptions on μ and $\tan \beta$. The

⁵Note that \tilde{M}_{N_i} can be any (among two) of the neutralinos, all these equations being symmetrical under neutralino mass permutations.

⁶NB another recent analysis of the neutralino system in the LHC context of gluino/squark cascade decays has been performed in ref. [42], also partly based on semi-analytic relations, though very different from ours and not relying on exactly the same input masses.

latter assumptions are anticipating the difficulty of determining $\tan \beta$ at the LHC solely from such cascade decay information, as will be confirmed more quantitatively in next sections. We thus illustrate the cases where both μ and $\tan \beta$ would be largely undetermined, and how the M_1, M_2 determination is improving if a more precise determination of μ and $\tan \beta$ can be available (anticipating the accuracies on $\tan \beta$ and μ that may be determined from other LHC processes, or alternatively if supplementing our analysis with ILC determination of parameters). One observes from Fig. 2 that for largely unknown $\tan \beta$ and μ the constraint obtained on M_1 from using solely the two neutralino mass input is fairly reasonable: $80 \text{ GeV} \lesssim M_1 \lesssim 120 \text{ GeV}$. In contrast M_2 is poorly constrained in this case (though there are two distinct branches appearing with a “gap” around $M_2 \sim 150$ approximately, where clearly only the upper part corresponds to SPS1a). Moreover only the region $M_2 \lesssim 400 \text{ GeV}$ is shown, while actually there are a few isolated points in the scan appearing for even much higher M_2 . We have checked that using a regular grid scan instead of random numbers does not significantly alter the contours in Figs. 2-3 or similar other figures as will be presented below. One should be careful in the interpretation of the density levels of various regions, since our scan was performed here with uniformly distributed random numbers. Accordingly the density levels of points as appearing in Fig. 2 principally reflect that the determination of M_1, M_2 from Eqs. (6)-(7) is very non-linear with respect to μ (and with respect to $\tan \beta$ to some extent), and have thus no direct meaning of statistical confidence levels. In next sections we will often make explicit comparisons between uniform and Gaussian scanning of parameters, where in the latter case statistical confidence levels may be more properly defined (with the cautions however mentioned in section 2.4 regarding the fact that the data errors used in the present work are not purely statistical anyway). In some cases the differences are significant and deserve a more careful analysis, as we will see.

The cases of moderate (blue region) and accurate (magenta region) determination of $\tan \beta, \mu$ is evidently giving much more interesting constraints. The case of $\Delta\mu \sim 15 \text{ GeV}$ is anticipating on the expected approximate accuracy on μ when a third neutralino can be measured, as will be analyzed in a next subsection. (Alternatively a better determination of μ is also obtained when the latter is not arbitrary as it is in a general MSSM but calculated from EWSB consistency conditions from universal Higgs and sfermion mass terms at the GUT scale, as will be analyzed in section 6.) Now, contour plots like those in Fig. 2 are not very informative as concerns the improvement in M_1 or M_2 determination to be expected when increasing either μ or $\tan \beta$ accuracy respectively. For example, there is not much differences between the constraints obtained for moderate $\Delta\mu = 100 \text{ GeV}$ accuracy and for tighter $\Delta\mu = 15 \text{ GeV}$ accuracy. The reasons for this will become clear from the next figure. To trace more clearly this behaviour we plot in Fig. 3 the equivalent of the green contour of Fig. 2 now in the (μ, M_2) and (μ, M_1) planes respectively. The spreading of points in these plots is due to the (wide) variation of $\tan \beta$ and of m_{N_1}, m_{N_2} . More precisely what is shown in red in the effect of m_{N_1}, m_{N_2} experimental errors only, for fixed SPS1a value of $\tan \beta = 9.74$, while the additional green points correspond to $1 < \tan \beta < 50$. These plots are thus essentially the solutions $M_{1,2}(\mu)$ from Eqs. (6)-(7), that would reduce to simple curves for fixed $\tan \beta, m_{N_1}, m_{N_2}$. One can see very clearly the different branches of solutions for (M_2, μ) (and correspondingly

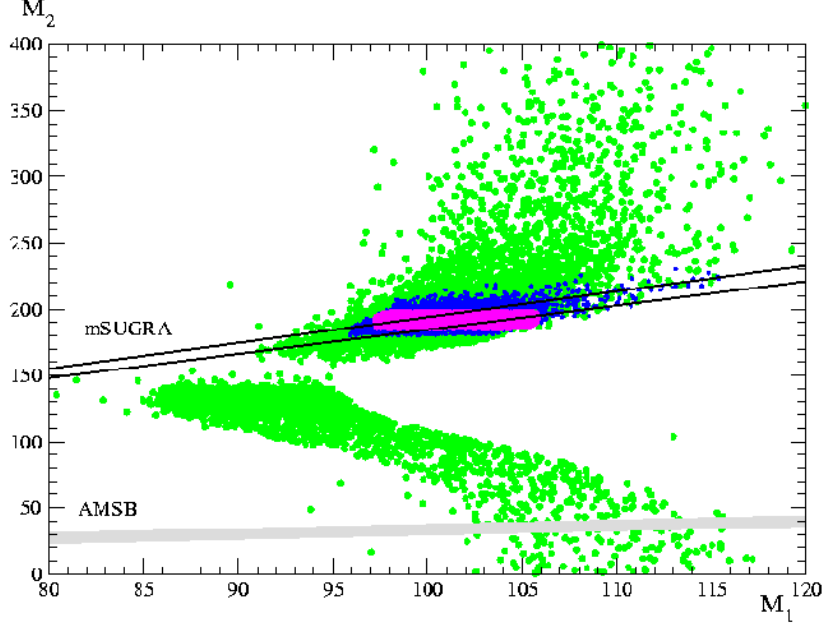


Figure 2: M_1, M_2 determination from two neutralino masses m_{N_1}, m_{N_2} in unconstrained MSSM for different assumptions on $\mu, \tan\beta$: 1) green: ($\tan\beta, \mu$ essentially unconstrained): $\mu = \mu(\text{SPS1a}) \pm 1 \text{ TeV}$, $1 \lesssim \tan\beta \lesssim 50$; 2) blue: (moderately constrained): $1 < \tan\beta < 50$, $\Delta\mu = 100 \text{ GeV}$; 3) magenta (well constrained): $\Delta\tan\beta = 2$, $\Delta\mu = 15 \text{ GeV}$. Also shown are the mSUGRA/GMSB (AMSB) M_1/M_2 relations in black (respectively in grey) including experimental errors on the masses.

(M_1, μ)), that originate from the fourth order in μ in Eqs. (6)-(7), with strong correlations. In fact $M_2(\mu)$ has two poles for $\mu < 0$ and $\mu > 0$ (which are not exactly symmetrical): for instance for SPS1a values of $\tan\beta, m_{N_1}, m_{N_2}$, the positive pole is at $\mu \sim 118 \text{ GeV}$. This explains the loose determination of M_2 for large variation of μ , and also explains the density levels of scanning points in Fig. 2. Conversely one can see that M_2 and M_1 can be much better constrained, irrespectively of $\tan\beta$ values, as soon as the μ determination is slightly better (such that μ remains sufficiently far from the poles). This explains the much improved constraints on M_2 and M_1 for the blue contour in Fig. 2. All these properties are rather simple consequences of the basic Eqs. (6)-(7), and illustrate useful informations that would be very difficult to delineate from a more standard top-down fit of parameters. One might argue that the pole is an artifact of our inversion equations, but more physically it simply reflects that it is not possible to get these m_{N_1}, m_{N_2} SPS1a values with a reasonable, finite M_2 , for such μ value. More precisely, going back to the top-down approach, performing e.g. a χ^2 fit of the neutralino masses will imply a flat behaviour of the χ^2 near this μ region, such that no clear minimum can be found and/or that the χ^2_{\min} value will be bad. This is

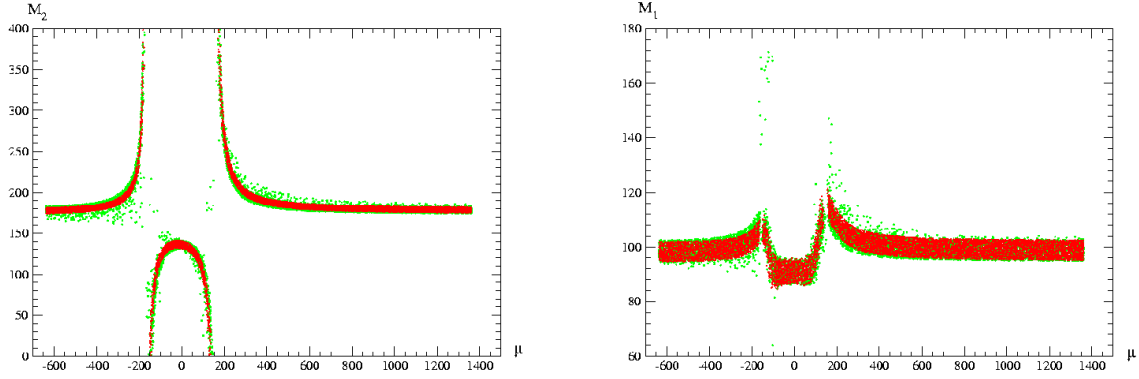


Figure 3: M_2 (left) and M_1 (right) as functions of μ . The spreading of points is due to the variation $1 < \tan \beta < 50$ (in green) as well as the variation of m_{N_1}, m_{N_2} within accuracy (in red).

fully confirmed by the results of a MINUIT fit as shown in Table 3: for fixed SPS1a values of μ (and $\tan \beta$) and fitting only m_{N_1}, m_{N_2} gives very good accuracy on M_1, M_2 :

$$M_1 = 108.8 \pm 5.8 \text{ GeV}, \quad M_2 = 208.9 \pm 6.4 \text{ GeV}. \quad (8)$$

In contrast, when μ is fixed to ~ 120 GeV the minimization does not give useful constraints, MINUIT finds typically errors like:

$$M_1 = 2000 \pm 258 \text{ GeV}, \quad M_2 = 2000 \pm 88 \text{ GeV}. \quad (9)$$

with even many similar other minima and errors found for very large M_2 value.

Next, if gaugino universality relations at the GUT scale are assumed, one obtains as expected stronger constraints. This is illustrated by the band resulting from the “mSUGRA” relation: $M_1 \simeq 0.53M_2$ at the relevant low energy scale $Q \simeq Q_{EWSB}$, from $M_1(Q_{GUT}) = M_2(Q_{GUT})$ universality at GUT scale. The width of this band results from the error on M_3 , i.e. $m_{\tilde{g}}$ determination. We will see in next subsection how to make this study more precise when the (mSUGRA) gaugino mass universality is assumed. We anticipate that given the neutralino and gluino mass accuracies (M_3 in particular), even for gaugino mass universality assumptions the constraints on μ will be mild, while those on $\tan \beta$ almost absent: indeed one can see on Fig. 2 that the “mSUGRA” band is compatible even with the green region where $\tan \beta$ (and μ) are essentially undetermined.

In addition, since the contours in Fig. 2 are valid for arbitrary gaugino masses, it is straightforward to superpose different gaugino mass relations, for instance in AMSB[43] models where the M_1/M_2 relation is also fixed from high scale boundary conditions and RG evolution, but is very different: $M_1(Q_{EWSB}) \simeq 2.9M_2(Q_{EWSB})$. We show similarly on Fig. 2 this ‘AMSB’ band (in grey) including its width originating from M_3 uncertainty. In this way one may possibly distinguish,

depending on the accuracy, between e.g. mSUGRA/GMSB and AMSB models from the neutralino mass measurements (however the relation between M_1 and M_2 in GMSB models[44] is completely indistinguishable from the mSUGRA relation at this accuracy level). More precisely one can see here how AMSB would be excluded if moderate (in blue) or accurate (in pink) $\tan \beta$ and μ measurements could be achieved. This is also a consistency cross-check, in the present analysis, since we started from a mSUGRA model SPS1a “data”.

3.2 Scenario S2: determining $\mu, \tan \beta$ with gaugino mass universality

In a next scenario we consider the very same basic Eqs. 6,7 but changing input/output: adding now the gaugino universality assumption: $M_1 = M_2 = M_3$ at the GUT scale, to first determine M_1, M_2 from M_3 . (This does not necessarily imply a mSUGRA model, as non-universal relations could still hold for all other MSSM parameters apart gaugino mass terms). At the one-loop level this universality relations read:

$$\frac{M_1}{g_1^2} = \frac{M_2}{g_2^2} = \frac{M_3}{g_3^2} \quad (10)$$

(where g_i are the properly normalized gauge couplings) to be valid at any scale. Numerically, this gives approximately at the relevant low energy EWSB scale:

$$M_1 \simeq 0.17M_3, \quad M_2 \simeq 0.33M_3, \quad M_1 \simeq 0.53M_2 \quad (11)$$

To determine M_1, M_2 from M_3 , one first extract M_3 from the the gluino pole mass $m_{\tilde{g}}$ as

$$m_{\tilde{g}}^{pole} = M_3(Q) + \Sigma_{\tilde{g}}(Q; m_{\tilde{q}}, \dots) \quad (12)$$

by subtracting out the leading radiative corrections $\Sigma_{\tilde{g}}$ to the gluino mass that are dominantly due to squarks, and thus largely predictable in our framework, as discussed above in section 2.3. This induces a non-negligible shift, since for SPS1a the correction $\Sigma_{\tilde{g}} \sim 20$ GeV, with $M_3(Q_{EWSB}) \sim 600$ GeV.

We next solve Eqs. (6), (7) as a linear system for $\sin 2\beta$ and μ^2 . Our conventions are the usual ones such that $0 < \beta < \pi/2$, so that $\tan \beta > 0$ (and real). This is not a restriction on parameter space, since eventual phase of $\tan \beta$ can be absorbed by a consistent redefinition of the Higgs doublet fields[23]. The sign of μ , however, is not determined by these equations, so we have to consider the two possible solutions for $\mu > 0$ and $\mu < 0$ a priori. As a cross-check we can as previously plug in these expressions the central SPS1a values for the masses $M_{\tilde{g}}, \tilde{M}_{N_1}, \tilde{M}_{N_2}$ as obtained e.g from SuSpect, obtaining the correct values of $\tan \beta$ and μ ⁷. Next we vary $M_{\tilde{g}}, \tilde{M}_{N_1}, \tilde{M}_{N_2}$ within accuracy according to Table 1. Scanning the values with (uniformly distributed) random numbers, with the conditions: μ real and $\tan \beta > 0$ is illustrated in Figs. 4–6. A number of remarks are

⁷Strictly speaking one should include here the theoretical uncertainties on \tilde{s}_W^2 as well, but the latter are rather small in comparison to the experimental uncertainties on the other parameters. Yet, this is related to the consistent inclusion of radiative corrections, which contribute to \tilde{s}_W^2 . In fact this induces a small shift of the central values but will affect very little the variation range of the output parameters M_1, M_2 here.

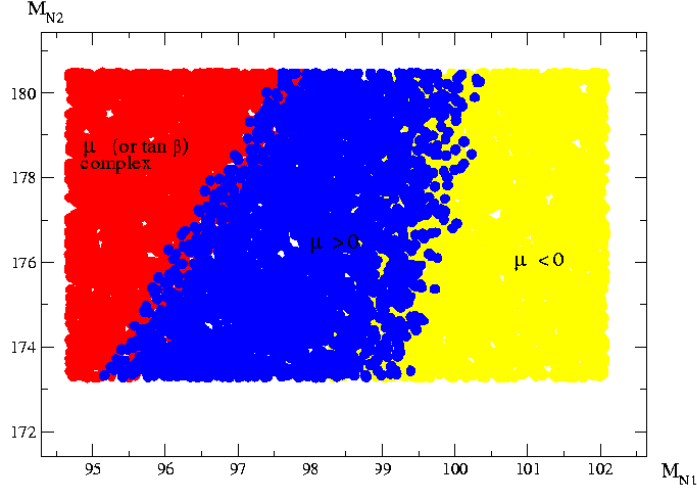


Figure 4: Allowed domain for \tilde{M}_{N_1} , \tilde{M}_{N_2} corresponding to complex or real μ .

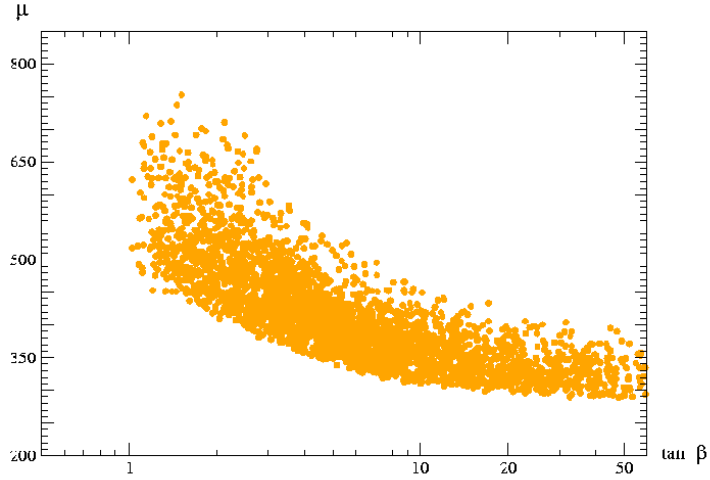


Figure 5: Constraints on $\mu > 0$, $\tan \beta$ from gaugino universality and gluino plus two neutralino mass measurements in gluino cascade decay.

worth here: first, requiring μ to be real *further* restrict the error on the neutralino masses, since the red domain in Fig. 4 is to be excluded. In the most general MSSM case, μ may have a non-zero phase, but if we restrict analysis to real parameter space this is an interesting additional constraint, resulting solely from the consistency of Eqs. (6), (7). The two other domains correspond to $\mu > 0$

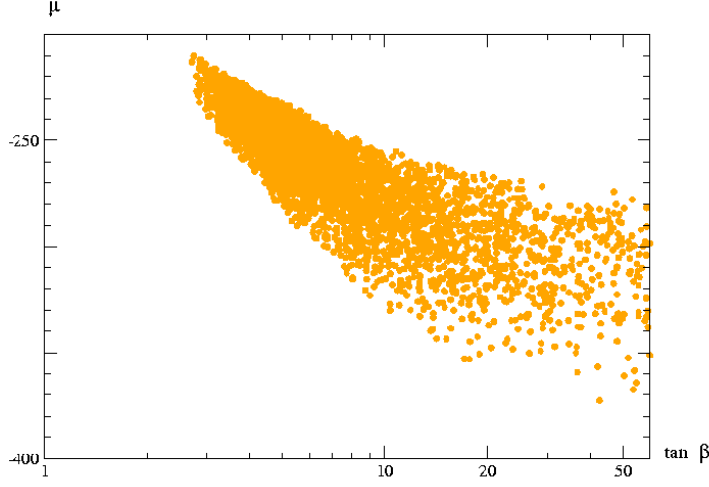


Figure 6: Constraints on $\mu < 0$, $\tan \beta$ from gaugino universality and gluino plus two neutralino mass measurements in gluino cascade decay.

and $\mu < 0$ respectively, so that the latter cannot be excluded given these SPS1a input accuracies on the two neutralino masses. If the latter mass accuracy could be reduced by a factor of about 2, the $\mu < 0$ solution would disappear altogether (as well as the complex μ possibility).

Next the corresponding constraint in the $\tan \beta, \mu$ plane are shown in Figs. 5 and 6 respectively for $\mu > 0$ and $\mu < 0$. We observe that $\tan \beta$ is practically unconstrained, especially for large $\tan \beta$, and $\mu > 0$ poorly constrained, given these accuracies on neutralino and gluino masses. Note however that for $\mu > 0$ the two parameters appear strongly correlated as the shape of the contour is showing: e.g. for $\mu > 0$ large $\mu \sim 600 - 700$ GeV is only possible for small $\tan \beta \sim 2$. This correlation is not an artifact of our simple random scan, but a simple consequence of the μ and $\sin 2\beta$ dependence within Eqs. (6), (7). More precisely we find:

$$\tan \beta \gtrsim 1, \quad 280 \text{ GeV} \lesssim \mu \lesssim 750 \text{ GeV} \quad (13)$$

for $\mu > 0$ and

$$\tan \beta \gtrsim 2.7, \quad 210 \text{ GeV} \lesssim |\mu| \lesssim 370 \text{ GeV} \quad (14)$$

for $\mu < 0$, and in both cases no upper limits on $\tan \beta$, which is clearly understandable because only $\sin 2\beta$ appears in any of the relations above in Eqs. (5–7)[19], so that for large $\tan \beta$ any sensitivity on $\tan \beta$ disappears.

These results are thus consistent with what was anticipated from the previous analysis illustrated in Fig 2, where the gaugino “mSUGRA” universality band is crossing all domains of the chosen $\tan \beta, \mu$ range of variation, in particular the green region where $\tan \beta$ was essentially arbitrary. The fact that μ is better constrained for $\mu < 0$ is understandable from Fig. 4 where

the domain corresponding to $\mu < 0$ is smaller than the $\mu > 0$ one, moreover the central value $|\mu| \sim 357$ GeV is excluded on the plot Fig. 6 This is due to the fact that the SPS1a with $\mu > 0$ is the right solution, but without knowing the true SPS1a value of μ we could not exclude $\mu < 0$ solutions from solely these cascade decay measurements.

3.3 Scenario S3: $\mu, \tan \beta$ from three neutralino with universal gaugino masses

What could be more constraining is the (more optimistic) scenario where three neutralino masses could be determined from the former gluino cascade Eq. (1) together with another squark decay measurement (independent from the first gluino cascade decay)[5], according to the input S_3 in Table 1 above. In this case one can use very simply an extra (linear) relation originating from Eqs. 5 to get a more precise determination of μ and $\tan \beta$ under similar other assumptions. This is illustrated in Fig. 7, where one observes that the $\mu < 0$ solution has disappeared (and the equivalent of Fig. 4 would show that only a smaller part of the red contour $\mu > 0$ is surviving). However, only μ is much more constrained, while apart from a more interesting lower bound $\tan \beta$ remains essentially unconstrained for large $\tan \beta$, which is simply due to the $\sin 2\beta$ only dependence in all these relations, whatever the number of input neutralino masses. More precisely:

$$\tan \beta \gtrsim 2.7, \quad 350 \text{ GeV} \lesssim \mu \lesssim 372 \text{ GeV} \quad (15)$$

These results are consistent with general expectations that the gaugino sector alone can hardly constrain $\tan \beta$ at the LHC, even in the mSUGRA (gaugino universality) case, but these features are perhaps very simply illustrated here analytically.

Concerning the inclusion of radiative corrections into this essentially tree-level determination, we have already mentioned the use in all these relations of the \overline{DR} parameters \bar{s}_W^2, \bar{m}_Z , which already incorporate a part of the corrections. The bulk of these \overline{DR} corrections with respect to tree-level values come from standard model contributions, and supersymmetric contributions, though not negligible, are inducing strictly speaking some theoretical uncertainties if the virtual contributions from unknown sector are taken into account. Next the corrections from the running to the pole neutralino masses remain moderate in the MSSM so that one may neglect them in a first approximation. Actually, most of these radiative corrections can be incorporated in the form of correction to the “bare” parameters μ, M_1, M_2 to very good approximation[38], while off-diagonal corrections to e.g. the neutralino mass matrix are smaller[38]. In this way our procedure to determine e.g. M_1, M_2 or μ above remain correct up to an implicit shift on these parameters (provided one has some knowledge on the corrections). In fact gluino mass corrections are dominantly due to squarks/quark, and quite similarly for neutralinos, so they can be evaluated within a reasonable approximation without assuming more knowledge than the available cascade decay input. As discussed in section 2.3, though it is not completely straightforward to incorporate consistently all these corrections within these parameters, it is very similar to the kind of iterative procedure required for a standard top-down calculation of MSSM spectrum[31]. This is taken into account in the illustrations shown here.

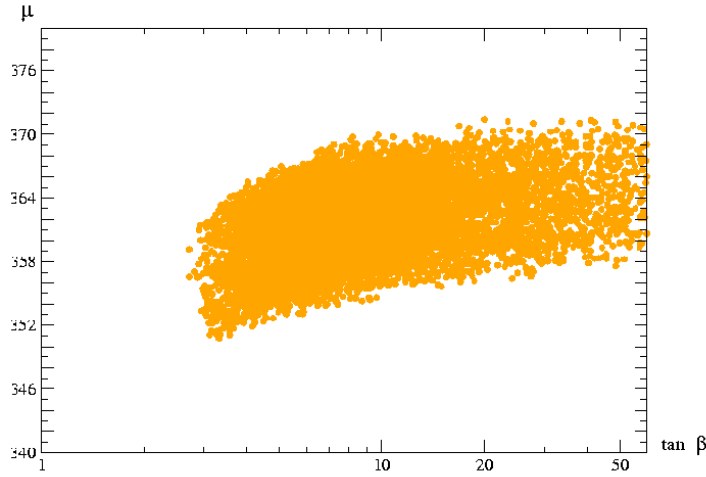


Figure 7: Constraints on μ , $\tan \beta$ from gaugino universality and gluino plus three neutralino mass measurements in gluino + squark cascade decay.

Next, to cross-check the above analytical determination we perform alternatively standard top-down χ^2 minimization fits, using MINUIT. The best fit and error results in the gaugino mass universality case (but assuming an otherwise general MSSM scenario i.e. with μ arbitrary) are shown in Table 3 both for two and three neutralino mass input. As one can see the fit results are overall consistent with our analytical determination, though the symmetrical (MIGRAD) minimization does not reflect the very unsymmetrical behaviour of the parameters, most notably for $\tan \beta$ and μ . Indeed the unsymmetrical non-linear MINOS minimization does not give any useful constraint for $\tan \beta$. The rather bad constraints obtained for the non-universal gaugino mass case when μ and $\tan \beta$ are varied in a wide range, are consistent with the above analysis of the μ dependence of M_2 and M_1 illustrated in Fig. 3, as already discussed above.

3.4 Reconstructing gaugino masses at GUT scale

As shown in Table 3 the constraints on M_1 , M_2 can be very good if μ and $\tan \beta$ are close to their nominal SPS1a values. Note that there is very little improvement on M_1 , M_2 accuracy if using the third neutralino mass input $m_{\tilde{N}_4}$. The M_1 and M_2 errors are changed to 5.7 and 6.3, respectively. In contrast the improvement on μ was very substantial, as can be seen both in Fig. 7 and Table 3. This is explained by the fact that for SPS1a $m_{\tilde{N}_1}$, $m_{\tilde{N}_2}$ are essentially Bino-like and Wino-like respectively, while $m_{\tilde{N}_4}$ is essentially Higgsino-like.

Finally we perform bottom-up RGE for these parameters in the non-universal case in order to check eventually for gaugino mass unification at a high GUT scale, following ref. [21]. (NB the bottom-up RGE of gaugino masses and all other basic MSSM parameters from given values at

Table 3: Constraints on gaugino-Higgsino sector parameters from a standard top-down χ^2 MINUIT fit of neutralino and gluino masses under universal or non-universal gaugino mass assumptions.

Data & fitted parameter (+ model assumptions)	MIGRAD (68%C.L.)	MINOS (68%C.L.)	nominal SPS1a value
$m_{\tilde{N}_1}, m_{\tilde{N}_2}, m_{\tilde{g}}$ (1-loop RGE + no \tilde{q} R.C) (Non-universal M_i)			
M_1	108.6 ± 58		108.8
M_2	208.6 ± 181		208.9
μ	340.9 ± 186		340.6
$\tan \beta(Q_{EWSB})$	10.6 ± 36		9.74
M_1	108.8 ± 5.8		108.8
M_2	208.9 ± 6.4		208.9
μ	341 (fixed)		340.6
$\tan \beta(Q_{EWSB})$	9.74 (fixed)		9.74
(Universal $M_i(Q_{GUT})$) $m_{\tilde{N}_1}, m_{\tilde{N}_2}, m_{\tilde{g}}$ (1-loop RGE + no \tilde{q} R.C)	(convergent)	(problems)	
M_3	603.8 ± 13.5	603.8 ± 13.5	603.8
μ	341.6 ± 293	341.6 ± 293	340.6
$\tan \beta(Q_{EWSB})$	9.73 ± 52.6	(not calculated)	9.74
$m_{\tilde{N}_1}, m_{\tilde{N}_2}, m_{\tilde{N}_4}, m_{\tilde{g}}$ (1-loop RGE + no \tilde{q} R.C)	(convergent)	(problems)	
M_3	603.8 ± 13.4	603.8 ± 13.4	603.8
μ	340.6 ± 13	340.6 ± 13	340.6
$\tan \beta(Q_{EWSB})$	10.0 ± 15.3	(not calculated)	9.74

EWSB scale is illustrated in some details in Appendix). This is shown in Figs. 8 for the minimal errors above and in 9 for the worst errors. One can see that a very good check of GUT scale universality is possible as long as the initial M_i accuracies are reasonable: in other words, the error dispersion from gaugino mass RGE remains small, which is clearly explained by their RGE content (typically the fact that they only depend on gauge coupling at the one-loop level). As expected this is qualitatively consistent with the former results of ref. [21] (though it appears that the M_1, M_2 LHC accuracies considered at that time were slightly more optimistic than the ones we obtained from our analysis). The dispersion from bottom-up RGE will be more important for other parameter sectors, in particular for the m_{H_u} parameter in the Higgs sector as is well-known (see the discussion and illustrations in Appendix). Nevertheless, even for gaugino masses the possibility of checking universality at GUT scale may become elusive in the extreme case where

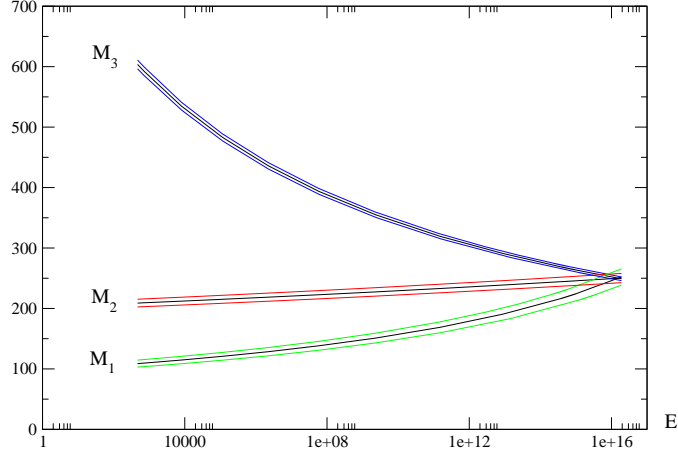


Figure 8: Bottom-up RGE of gaugino masses from EWSB to GUT scale, including error propagations (μ and $\tan \beta$ are fixed to their SPS1a values).

almost nothing is known on μ , such that the M_1 , M_2 low scale values errors are large, and only M_3 error remains under control, as illustrated in Fig. 9. We also remark once more that in addition to performing bottom-up RGE, mSUGRA gaugino universality could be checked usefully from plots as illustrated in Fig. 2 (where it can also be eventually distinguished from other high scale SUSY-breaking models like AMSB).

4 Squark/slepton parameter determination (first two generations)

We will now try to determine constraints on the (first and second generation) squark and/or slepton sector parameter of the MSSM from the cascade decay with the expected accuracy on the masses of \tilde{q}_L and \tilde{l}_R from Table 1. As already mentioned in section 2, there is at present no way to tag the charge and flavor of the relevant (first two generations) squark at LHC so that different flavor should be combined. Accordingly the resulting mass accuracies of say, an up or down squark, are assumed to be identical[4], so that there is no need to combine their errors in a statistically elaborated manner, and we thus assume that it is sufficient for our purpose to take the average of two (identical) errors in our analysis. Concerning the model assumptions, we shall consider two different scenarios, in a general unconstrained MSSM and in a constrained MSSM with universality of slepton and squark masses.

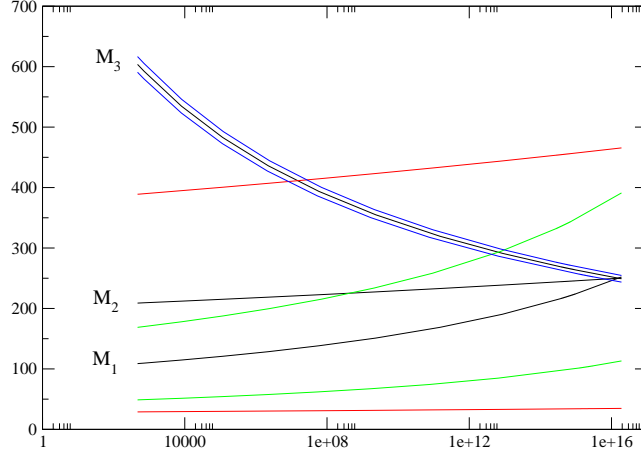


Figure 9: Bottom-up RGE of gaugino masses from EWSB to GUT scale, including error propagations for the worst case (μ and $\tan \beta$ undetermined).

4.1 Unconstrained MSSM and a simple squark/slepton mass sum rule

The masses of the sparticles $\tilde{q}(\neq \tilde{b}, \tilde{t})$ and \tilde{l} participating in the cascade decay in Eq. (1) obey (at the EWSB scale) well-known relations (at tree-level) e.g for the up squark and selectron:

$$\begin{aligned} m_{\tilde{u}_1}^2 &= m_{\tilde{u}_L}^2 + \left(\frac{1}{2} - \frac{2}{3}s_W^2\right)m_Z^2 \cos 2\beta \\ m_{\tilde{e}_2}^2 &= m_{\tilde{e}_R}^2 - s_W^2 m_Z^2 \cos 2\beta \end{aligned} \quad (16)$$

which are valid in the general MSSM⁸. Similar relations for the other squark and slepton flavors. Eqs. (16) simply relate the physical masses to the soft breaking scalar masses via the additional D-terms. These relations are particularly simple for the first two squark and slepton generations due to negligible mixing. The main idea is to consider specific linear combination (“sum rules”) in order to eliminate the $\tan \beta$ dependence:

$$s_W^2 m_{\tilde{u}_1}^2 + \left(\frac{1}{2} - \frac{2}{3}s_W^2\right)m_{\tilde{e}_2}^2 = s_W^2 m_{\tilde{u}_L}^2 + \left(\frac{1}{2} - \frac{2}{3}s_W^2\right)m_{\tilde{e}_R}^2. \quad (17)$$

Taking into account the available accuracy on the physical masses $m_{\tilde{u}_1}$ and $m_{\tilde{e}_2}$ provides constraints on the MSSM soft-breaking scalar parameters $m_{\tilde{u}_L}, m_{\tilde{e}_R}$ *independently* of $\tan \beta$ values: So that even if $\tan \beta$ is largely undetermined (as is the case from the neutralino sector alone in previous section), Eq. (17) gives a (model-independent) determination of the linear combination of basic parameters which will be roughly of the order of magnitude of the mass accuracy itself,

⁸ s_W^2 in Eq. (16) and further equations below should be understood as the \overline{DR} -scheme parameter \overline{s}_W^2 .

i.e. a few percent. More precisely, a straightforward calculation from the experimental accuracy in Table 1 gives a $\sim 2.3\%$ ($\sim 2\%$) relative accuracy for the linear combination in Eq. (17), if we combine the $m_{\tilde{u}_1}$ and $m_{\tilde{e}_2}$ errors linearly (quadratically), respectively. (NB neglecting at the moment for simplicity the error on \bar{s}_W^2 : the effect of \bar{s}_W^2 uncertainties will be studied below). Another advantage of this linear combination is that, even in the unconstrained MSSM case, the RG evolution of the relevant parameters ($m_{\tilde{u}_L}(Q)$, $m_{\tilde{e}_R}(Q)$) depends only on the gauge couplings g_i and the gaugino masses M_i ⁹. The linear combination Eq. (17) can thus be RG-evolved within a restricted set of input parameters solely determined from the gluino cascade, in order to obtain the soft scalar term values at the GUT scale where one may check for eventual universality relations. It is clear that before doing this RG evolution, one has to subtract out radiative corrections linking the running to the pole masses, which are not negligible for squarks, in the way discussed in section 2.3. Concretely we have

$$M_{\tilde{u}_1}^{pole} = m_{\tilde{u}_1}(Q) + \Delta m_{\tilde{u}_1}(Q, m_{\tilde{q}}, m_{\tilde{g}}, \dots) \quad (18)$$

where these corrections are largely dominated by squark/gluino contributions at one-loop. For SPS1a we have $\Delta m_{\tilde{u}_1}(Q_{EWSB}, m_{\tilde{q}}, m_{\tilde{g}}) \sim 19$ GeV, which can be consistently subtracted out (involving some iterations) to define the running mass $m_{\tilde{u}_1}$. Concerning radiative corrections linking the running to the pole slepton mass, they are small and we shall neglect them in our analysis. Next, it is a straightforward exercise to work out the RG evolution of the linear combination (17):

$$\begin{aligned} \frac{d}{dt} \left[s_W^2 m_{\tilde{u}_L}^2 + \left(\frac{1}{2} - \frac{2}{3} s_W^2 \right) m_{\tilde{e}_R}^2 \right] = & s_W^2 \frac{dm_{\tilde{u}_L}^2}{dt} + \left(\frac{1}{2} - \frac{2}{3} s_W^2 \right) \frac{dm_{\tilde{e}_R}^2}{dt} \\ & + \frac{ds_W^2}{dt} \left(m_{\tilde{u}_L}^2 - \frac{2}{3} m_{\tilde{e}_R}^2 \right) \end{aligned} \quad (19)$$

where $t \equiv \ln Q$ and the standard RG evolution of the relevant parameters $\tilde{m}_{u_L}^2$, $\tilde{m}_{e_R}^2$ is used (which as mentioned only depend on g_i , M_i). We also have:

$$\frac{ds_W^2}{dt} = \left(\frac{3}{5} g_1^2 + g_2^2 \right)^{-1} \left(\frac{3}{5} c_W^2 \frac{dg_1^2}{dt} - s_W^2 \frac{dg_2^2}{dt} \right) \quad (20)$$

with $s_W^2(t) \equiv \frac{3}{5} g_1^2(t) / (\frac{3}{5} g_1^2(t) + g_2^2(t))$ and the factor $3/5$ is due to the standard normalization of the $U(1)_Y$ coupling g_1 in the MSSM RGE. Eqs. (19) and (20) take into account the RG evolution of \bar{s}_W^2 (which is not at all negligible since it is related to the gauge coupling which are evolving substantially from m_Z input values to GUT values).

Like for the gaugino masses in the previous section, the bottom-up RG evolution of MSSM parameters can be performed with a specific SuSpect option. As already mentioned one important feature of this bottom-up RG evolution is that some of the low scale parameter uncertainties are

⁹This is only true strictly speaking at the one-loop level RGE, since at two-loop level practically all MSSM parameters enter the RG evolution of squark and slepton mass terms[26, 27]. We shall discuss below how the inclusion of two-loop RGE effects affect our results, but we anticipate that neglecting these higher loop effects do not change drastically the obtained constraints.

amplified once evolved to a large scale, depending on the structure of RG beta functions for some of the relevant parameters, and this amplification arises to some extent with the evolution of Eq. 17, as we will see later.

4.2 Constrained MSSM with squark, slepton universality

If we now assume squark and slepton mass universality at the GUT scale, Eq. (19) immediately determines $m_0^{q,l}(Q_{GUT})$:

$$s_W^2 m_{\tilde{u}_L}^2 + \left(\frac{1}{2} - \frac{2}{3}s_W^2\right)m_{\tilde{e}_R}^2(Q_{GUT}) \equiv \frac{5}{8}(m_0^{q,l})^2 \quad (21)$$

where the gauge coupling universality relation at the GUT scale: $s_W^2(t = \ln Q_{GUT}) = 3/8$ has been used. $m_0^{q,l}$ indicates that we only assume universality for the (first two generation) squark and slepton sector at this stage, i.e. not necessarily for the third generation sfermion nor Higgs scalar terms like in mSUGRA models. Now by combining accuracies on the measured \tilde{u}_1 and \tilde{e}_2 masses in Table 1, we obtain:

$$84 \text{ (86) GeV} \lesssim m_0^{q,l} \lesssim 116 \text{ (112) GeV} . \quad (22)$$

Note that the first limits are for linearly combined mass uncertainties (while those in parenthesis are for quadratically combined mass uncertainties). We emphasize that the bounds in Eq. (22) are independent of $\tan \beta$ values. However, there is a rather important amplification of the initial low scale uncertainty $\sim 2\%$ due to error propagation in the bottom-up RG evolution, and because of the additional terms proportional to ds_W^2/dt in Eq. (19). To trace in more details the origin of these resulting m_0 uncertainties let us take into account only one of the two squark, slepton mass uncertainty at a time, this gives

$$86.6 \text{ GeV} \lesssim m_0^{q,l}(\Delta m_{\tilde{u}_1}) \lesssim 112 \text{ GeV} \quad (23)$$

and

$$97.1 \text{ GeV} \lesssim m_0^{q,l}(\Delta m_{\tilde{e}_2}) \lesssim 103 \text{ GeV} \quad (24)$$

respectively. Thus the final uncertainty on m_0 is largely dominated by the $m_{\tilde{u}_1}$ uncertainty. Actually, the latter bounds on $m_0^{q,l}$ were calculated for fixed gaugino mass terms M_i . But since the RG evolution of $m_{\tilde{u}_L}, m_{\tilde{e}_R}$ depends on gaugino masses, the $m_0^{q,l}$ accuracy should be sensitive to M_i uncertainties, mainly those of M_3 which are enhanced in the $m_{\tilde{u}_L}$ RGE by the strong coupling: $dm_{\tilde{u}_L}^2/dt \sim -\frac{8}{3\pi}\alpha_S M_3^2$ [26, 27]. This leads to an important amplification of $m_0^{q,l}$ final uncertainty due to the $\Delta M_3 \sim 7 \text{ GeV}$ uncertainty (although the latter effect is damped somehow by $\bar{s}_W^2 \sim .238$ in the first term in the second member of Eq. (19), while other terms in Eq. (19) are not much sensitive to M_i uncertainties). One thus obtains, in the conservative case of uncorrelated and linearly combined errors, a maximal uncertainty on $m_0^{q,l}$ of about $\pm \sim 32 \text{ GeV}$ (respectively $\pm \sim 22 \text{ GeV}$ when combining errors quadratically) instead of the bounds shown in Eqs. (22)–(24)¹⁰. Now it is

¹⁰Note also that the dominant uncertainties from $m_{\tilde{u}_1}$ and $m_{\tilde{g}}$ (i.e. M_3) have the opposite (anti-correlated) effect: from the RG structure, increasing (resp. decreasing) $m_{\tilde{u}_1}$ makes $m_0^{q,l}$ to increase (resp. decrease), while the opposite behaviour occurs for $M_3 \pm \Delta M_3$.

clear that the linear combination Eq. (17) does not use the full information from the two independent mass relations in Eq. (16). We shall illustrate below how this additional information improves rather substantially the limits on $m_0^{q,l}$.

Another potentially interesting question is whether we can derive at the same time any useful limits on $\tan\beta$ once using the complete information from both squark and slepton masses. At first sight one may naively expect to obtain some upper bounds on $\tan\beta$ since the relations (16) are sensitive to $\cos 2\beta$. However a simple estimate immediately indicates that interesting $\tan\beta$ upper bounds from this squark, slepton sector are hardly expected for the given LHC \tilde{e}_2, \tilde{u}_1 mass accuracies: in fact for the SPS1a point with $\tan\beta(Q_{EWSB}) \sim 9.74$, $\cos 2\beta \sim -0.979$ i.e. very close to -1 , so that one would need at least an accuracy $\lesssim 0.02$ on $|\cos 2\beta|$ to put useful upper limits on $\tan\beta$. In contrast, a simple calculation of uncertainties from both Eqs. (16) gives:

$$\Delta|\cos 2\beta| \sim 0.6 \quad (25)$$

even in the optimistic case where we combine the $m_{\tilde{u}_1}, m_{\tilde{e}_2}$ uncertainties quadratically, and neglect the errors on s_W^2 . The above estimate, however, does not take into account other possible constraints on $\tan\beta$, that may come from other sectors, or from theoretical consistency. For instance the obvious constraint $|\cos 2\beta| \leq 1$ put additional limits on $m_{e_R}^2 - m_{e_L}^2$ via Eqs. (16), so indirectly on $m_0^{q,l}$. (This is quite similar to the extra constraints obtained in the neutralino sector in previous section from requiring μ to be real). Furthermore for $m_0^{q,l} \sim 100$ GeV it is easily checked that $\tan\beta$ cannot be larger than $\tan\beta \lesssim 35 - 36$, as beyond this value a tachyonic mass for the lightest stau $m_{\tilde{\tau}_1}$ occurs due to the stau mixing $\tilde{m}_\tau \cdot \mu \tan\beta$ term. Moreover the lightest Higgs mass becomes inconsistent or too low for small $\tan\beta \lesssim 2.2$ approximately, and for low $\tan\beta$ values the LEP lower bounds on m_h [45] actually put a tighter constraint $\tan\beta \gtrsim 8 - 9$. Yet the latter limits are theoretical and model-dependent (or experimental and model-dependent in the case of m_h bounds) but anyway tightly bound to the SPS1a benchmark[34], which was chosen on purpose to pass present experimental constraints. If we push $m_0^{q,l}$ sufficiently above the SPS1a central values, the upper bound $\tan\beta \lesssim 35$ from tachyonic $\tilde{\tau}_1$ is easily evaded, though in this case one should also take into account the lower bound $m_{\tilde{\tau}} \gtrsim 104$ GeV from LEP limits[46]. (For example, for $m_0 \sim 200$ GeV $\tan\beta \sim 50$ is not excluded by tachyonic stau, while the phenomenology from gluino, squarks cascade decays would not be drastically different from the SPS1a one). Similarly the $\tan\beta$ lower bound due to LEP m_h lower limits could easily be evaded in an unconstrained MSSM[47]. In any case we will not apply such direct (or indirect) experimental limits that would be to some extent dependent on the specific SPS1a choice, since our main aim is to present a reconstruction strategy expected to be valid beyond this particular benchmark choice.

Accordingly a question that we would like to examine in some detail here is whether the sole $m_{\tilde{u}_1}, m_{\tilde{e}_2}$ mass measurements could put some extra *model-independent* limits on $\tan\beta$. From the previous estimate it appears that to obtain stringent such experimental constraints on $\tan\beta$, one would require an accuracy about an order of magnitude better on the squark and slepton masses than the one prospected at the LHC. Incidentally this is roughly the accuracy expected at the ILC (though only for the sleptons), where both l_R and l_L masses could be measured at the per mille

level[5, 6]. However, a detailed ILC analysis is beyond the scope of the present paper and left for future work.

We anticipate that (model-independent) limits on $\tan \beta$ will be indeed absent or very marginal if using solely the first two generation squark and slepton mass accuracies. This is consistent with general prospects[5, 23]. We found however useful to examine this issue in some details, since our construction is not limited to the LHC mass accuracies here considered, and tracing analytically the sensitivity on parameters can help to understand better what precisely determine constraints in a more elaborated analysis.

To begin, there is a subtlety that is not taken into account in the above crude estimate of error combination in Eq. (25), such that it may underestimate the $\tan \beta$ sensitivity: as emphasized previously the RG equations for $m_{\tilde{u}_L}, m_{\tilde{e}_R}$ only depend on gauge couplings and gaugino masses, so in particular do not depend on $\tan \beta$ (at one-loop level). But there is in fact an indirect dependence on $\tan \beta$ even at one-loop (though very moderate): it originates from the boundary conditions on the RGE, namely the initial values of gauge couplings g_i in the \overline{DR} scheme, as well as their values at the GUT scale (if gauge unification is imposed), depend slightly on $\tan \beta$ through radiative corrections (see e.g. ref. [38]). Although these effects are strictly speaking small higher order corrections on $g_i(m_Z), g_i(m_{GUT})$ values, they are enhanced when running parameters from low to high GUT scale over more than 13 orders of magnitude, and most realistic calculations of MSSM spectra do take into account this dependence consistently[28, 29, 30, 31]. Moreover these values are notoriously different if using the RGE at the full two-loop level, or in a one-loop approximation, as will be illustrated below. (This is somewhat similar to the impact of precise initial gauge couplings and RGE approximations on the GUT scale value $\sim 2 \cdot 10^{16}$ GeV). Moreover, the low energy EWSB scale at which all soft parameters are evaluated also depend in principle on $\tan \beta$ values, and more generally it is not fixed by first principles: in most analysis the default EWSB scale is often fixed to $Q_{EWSB} \sim (m_{\tilde{t}_1} m_{\tilde{t}_2})^{1/2}$ (which is known to minimize the scale dependence[48] of the MSSM one-loop effective scalar potential). For the SPS1a point this is a well-defined value, but if relying only on the gluino cascade decay data, the stop masses are not assumed to be known in a general MSSM case. Thus we can in principle vary this EWSB scale, which can affect the final value of soft scalar masses, since this scale determines the end of the RG evolution. In our calculation we use either a fixed value (close to the true SPS1a for definiteness), or adopt the above default value in universality cases. In fact $m_{\tilde{u}_L}$ is expected to be specially sensitive to such variation due to the large coefficient $\sim \alpha_S M_3^2$ within its RGE, which makes it to run much faster than $m_{\tilde{e}_R}$. (E.g. for SPS1a $m_{\tilde{u}_L}(Q_{GUT}) = 100$ GeV evolves to $m_{\tilde{u}_L}(Q_{EWSB}) \sim 560$ GeV.)

For illustration in Fig. 10 we vary $m_{\tilde{u}_L}(Q_{EWSB})$ as function of $\tan \beta$, at one- and two-loop RGE order, both with fixed and default EWSB scale, using SuSpect 2.41. The variation with $\tan \beta$ is less than 2 GeV for $m_{\tilde{u}_L}$ (and we checked that it is completely negligible for $m_{\tilde{e}_R}$) for the whole $\tan \beta$ theoretically allowed range. This is accordingly below the prospected LHC accuracy on $m_{\tilde{u}_L}$ and so rather negligible for our analysis. In contrast there is a large difference between one and two-loop RGE, but this is usual for the whole MSSM spectrum as it is well known. This illustrates that for such reconstruction (or in fact any other kind of fits) one should be careful to

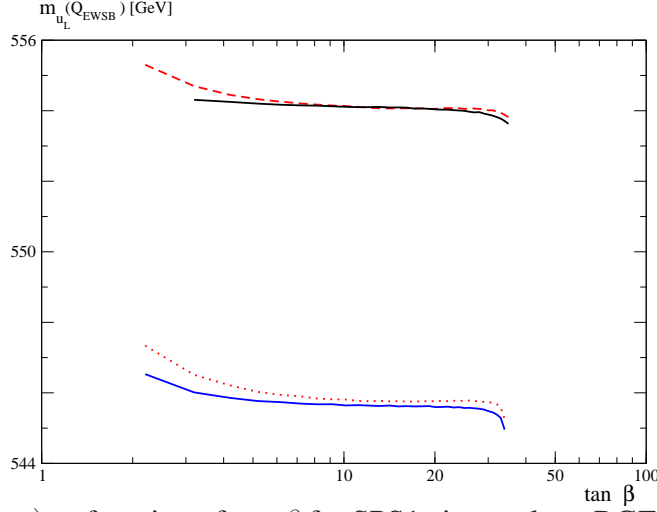


Figure 10: $m_{\tilde{u}_L}(Q_{EWSB})$ as function of $\tan \beta$ for SPS1a in one-loop RGE (top plots) and two-loop RGE (bottom plots). Red dashed line: one-loop RGE, default $Q_{EWSB} = (m_{\tilde{t}_1} m_{\tilde{t}_2})^{1/2}$. Black line: fixed $Q_{EWSB} = 468$ GeV. Orange dotted line: two-loop RGE, default $Q_{EWSB} = (m_{\tilde{t}_1} m_{\tilde{t}_2})^{1/2}$. Blue line: fixed $Q_{EWSB} = 468$ GeV.

be consistent with the RGE approximation used. Concerning now the small $\tan \beta$ dependence it should be kept in mind that any more elaborated fit (as could be performed from a χ^2 minimization using MINUIT) will be eventually sensitive to such effects, since these cannot be easily “switched off” from the fitting procedure. Moreover, such indirect dependence on $\tan \beta$ will be relevant anyway once reaching a better accuracy on slepton masses as is prospected e.g. at the ILC.

All these features are examined more quantitatively from a systematic scan over parameters, where we took into account the propagation of $m_{\tilde{u}_1}, m_{\tilde{e}_2}$ uncertainties in both relations (16) after evolving from low to high scale and back. More precisely we scanned over allowed mass bounds, considering the two mass uncertainties as independent (and uncorrelated) for simplicity. We also took into account any additional small dependence e.g. on $\tan \beta$ such as the one illustrated in Fig. 10. The $(m_0^{q,l}, \tan \beta)$ distributions obtained are shown first in Fig. 11 (the scan was performed with 3000 uniformly distributed random numbers). Comparing with Eq. (22) one notes that the lowest values of $84 \lesssim m_0 \lesssim 94$ GeV have been excluded simply from the constraint $|\cos 2\beta| < 1$. However, arbitrary large values of $\tan \beta$ are possible (provided that a sufficiently large number of scan points are taken), confirming the simple error estimate above in Eq. (25). The fact that large values of $\tan \beta$ are very few in Fig. 11, while low $\tan \beta$ values appear very much favored, is actually an artifact of the (uniform) scanning procedure where we basically scanned over the $m_{\tilde{u}_1}, m_{\tilde{e}_2}$ masses, which determine $\cos 2\beta$ via Eq. (16) rather than $\tan \beta$. So the distribution of points in Fig. 11 is simply resulting from the transformation from $\cos 2\beta$ to $\tan \beta$ and has not much statistical meaning as “most likely” values of $\tan \beta$. As already mentioned we shall refrain

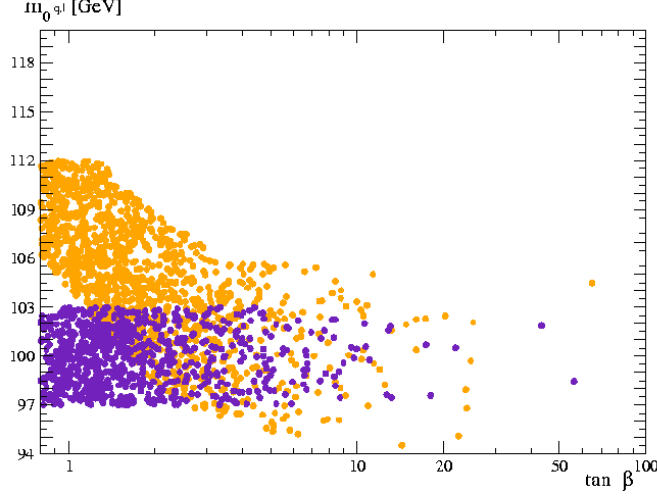


Figure 11: Constraints on $m_0 \equiv m_0^{q,l}$ and $\tan \beta$ from first two generation squark and slepton in gluino cascade decays after bottom-up RG evolution. The orange (respectively magenta) points correspond to constraints obtained from the squark $m_{\tilde{u}_1}$ (respectively $m_{\tilde{e}_2}$) relations in Eqs. (16).

to enter into a fully realistic statistical treatment of uncertainties, which would require to take into account[17], among other things, the non-trivial correlations implied by the cascade decay mass measurements. It is yet tempting in the present case to proceed one step further with a little more elaborated analysis. We thus perform a different scan, where instead of uniformly distributed “flat prior” random numbers, we exploit simple trigonometric relations to match more faithfully the true $\tan \beta$ distribution. In addition we start with Gaussian-distributed random numbers (assuming thus that the two independent errors are purely statistical, which is actually not really correct[3, 4]). We then calculate a “theoretical” χ^2 (where $\chi_{min}^2 = 0$ trivially since we use the correct central values of the masses) just to obtain well-defined confidence levels (C.L.) for the (joint) estimation of the two parameters $m_0^{q,l}$ and $\tan \beta$, assumed to be independent and uncorrelated. The result of this Gaussian scan is shown in Fig. 12. What are actually plotted are allowed points from the $m_{\tilde{e}_2}$ and $m_{\tilde{u}_1}$ relations in Eq. (16), at one- σ (more precisely 68% C.L.) in black and *additional* two- σ (95%) C.L., illustrated in indigo and orange respectively. The distribution of those allowed points is now essentially uniform in $\tan \beta$ (though now the apparent concentration for relatively large $\tan \beta$ is purely an artifact of the logarithmic scale), in contrast with the previous plot in Fig. 11. More importantly, $\tan \beta$ is constrained by lower and upper bounds, but these essentially originate from the theoretical (model-dependent) constraints, that are indicated in red for large $\tan \beta$ and correspond to a tachyon $\tilde{\tau}_1$. (NB the white zone for $\tan \beta \lesssim 2.2$ corresponds to a very light m_h). More precisely we observe that even at the 68% C.L., values of $\tan \beta$ up to the theoretical SPS1a constraint $\tan \beta \lesssim 35$ are not excluded. Moreover one sees that the 95% C.L. additional points (indigo and orange) have only the effect of slightly enlarging the $m_0^{q,l}$ determination but not much influence on $\tan \beta$ determination. Thus a more realistic treatment of errors simply confirms our above crude estimate, indicating that no interesting model-independent upper limits on $\tan \beta$ can be derived from the prospected LHC squark and slepton masses accuracies.

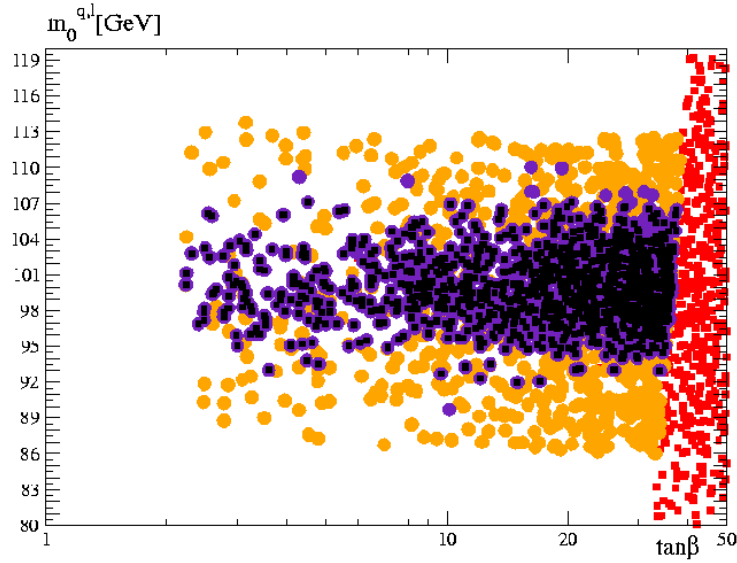


Figure 12: Constraints on $m_0 \equiv m_0^{q,l}$ and $\tan \beta$ with a scan over Gaussian random numbers: orange disks: 2- σ allowed points ($\chi^2 = \chi_{min}^2 + 6$) from $m_{\tilde{e}_2}$ relation; indigo disks: 2- σ allowed points from $m_{\tilde{u}_1}$ relation; black squared: 1- σ allowed points ($\chi^2 = \chi_{min}^2 + 2.3$) from $m_{\tilde{u}_1}$ relation. Red squared: excluded by tachyon $\tilde{\tau}_1$. (NB the square or disk sizes have no physical meaning).

It may be instructive to compare at this stage those results with a more standard top-down fit. We used MINUIT to perform a standard χ^2 minimization starting from a MSSM model with universal GUT $m_0^{q,l}$ and $\tan \beta$ free parameters. We first fix gaugino masses M_1, M_2, M_3 to SPS1a values and then fit this model to the “data” consisting of solely $m_{\tilde{u}_1}, m_{\tilde{e}_2}$. This two-parameter fit result is shown in Table 4 for different standard MINUIT minimization options, at the one- σ level. Actually the simpler MIGRAD[11] (symmetric error) minimization did converge, giving even a marginal upper limit at the one- σ level. This however does not give a very useful $\tan \beta$ bound, being above the theoretical $\tan \beta$ limits in this SPS1a case. On the other hand the more elaborated MINOS minimization, taking into account properly unsymmetrical errors and non-linearities[11], did not find any $\tan \beta$ upper (nor lower) limits. These results are thus qualitatively consistent with our more naive analysis above. Note that the m_0 bounds are also roughly consistent with our previous results. Now there are several reasons not to trust even the marginal upper bounds found for $\tan \beta$: though it is difficult to trace the very details of the minimization steps, the fit is much probably indirectly influenced by the $\tilde{\tau}_1$ becoming very small and ultimately tachyonic for $\tan \beta \gtrsim 35 - 36$: what happens more precisely is that, above those values SuSpect still gives $m_{\tilde{u}_1}, m_{\tilde{e}_2}$ output (unless explicit warning flags are switched on) but these are no longer very reliable (because the iterations needed to calculate a convergent spectrum are stopped in this case[31]). In particular, there is an abrupt change of $m_{\tilde{u}_L}$ once $\tan \beta \gtrsim 36$, see Fig. 10 (though the overall variation remains reasonable). Thus, comparing these minimization results and Fig. 12 with the simple estimate Eq. (25) we can infer that the marginal upper bound on $\tan \beta$ is principally deter-

Table 4: Constraints on $m_0, \tan \beta$ obtained from a standard top-down χ^2 fit with different model and input assumptions and different level of MINUIT minimizations.

Data & fitted parameter (+ model assumptions)	MIGRAD minimization (68%C.L.)	MINOS minimization (68%C.L.)	nominal SPS1a value
$m_{\tilde{e}_2}, m_{\tilde{u}_1}$ (1-loop RGE + no \tilde{q} R.C.) $m_0^{q,l}$ $\tan \beta$	(convergent) 99.98 ± 8.8 9.41 ± 29.8	$\tan \beta$ exceed limits 99.98 ± 8.7 9.41 ^{+no limits} ^{-no limits}	100 9.74
$m_{\tilde{e}_2}, m_{\tilde{u}_1} +$ $m_{\tilde{N}_1}, m_{\tilde{N}_2}, m_{\tilde{g}}$ (1-loop RGE + no \tilde{q} R.C.) $m_0^{q,l}$ $m_{1/2}$ $\tan \beta$	(convergent) 99.96 ± 7.9 250 ± 4.3 $10. \pm 29.8$	$\tan \beta$ exceed limits 99.9 ⁺¹⁰ ^{-10.5} 250 ± 4.3 10 ^{+29.8} ^{-no limits}	100 250 9.74

mined by the indirect small higher order $\tan \beta$ dependences, especially $m_{\tilde{u}_L}(\tan \beta)$ as illustrated in Fig. 10 originating mainly from the slightly varying EWSB scale, rather than directly from the $m_{\tilde{u}_1}, m_{\tilde{e}_2}$ accuracies. We have crosschecked this by redoing similar fits with a constant EWSB scale, or with two-loop RGE, which both have the effect of smoothing somewhat the variation of $m_{\tilde{u}_L}(\tan \beta)$ near the transition to tachyonic $\tilde{\tau}_1$ for $\tan \beta \sim 36$, and the $\tan \beta$ upper bound in Table 4 tends to increase (or even to disappear with non convergent minimizations). We have also further checked this by increasing progressively the mass accuracies: while the corresponding m_0 bounds decrease, following the expected statistical behaviour, for $\tan \beta$ one obtains either non convergent minimizations, or extra odd solutions far from the SPS1a values, and anyway no improvements on $\tan \beta$ bounds until a substantial decrease of these experimental errors is set (about an order of magnitude smaller than the LHC accuracies of Table 1).

For completeness we performed another fit taking into account in addition the neutralino and gluino masses with a three-parameter fit of $m_0, m_{1/2}, \tan \beta$. The situation does not improve much as concerns $\tan \beta$ limits, as illustrated by the corresponding results in Table 4. In this case the (unsymmetrical) MINOS m_0 bounds are slightly worse than for the two-parameter fit, which is expected since now M_3 is not fixed and correspondingly the M_3 accuracy propagates to the m_0 determination via the RGE, as explained above. On the other hand the accuracy on $m_{1/2}$ is very good. Finally we also performed a similar fit for a benchmark point like SPS1a except $m_0 = 200$ GeV, in which case the transition to tachyonic $m_{\tilde{\tau}_1}$ happens only for very large $\tan \beta > 50$, having thus potentially less influence on the fit. Assuming the same mass accuracies than for the true SPS1a point we obtain, for a two-parameter (respectively three-parameter) fit: $\tan \beta = 9.93 \pm$

52.2 (respectively $\tan\beta = 10.1 \pm 50.7$), at one- σ level, while errors for m_0 and $m_{1/2}$ are very comparable to the SPS1a ones. So this confirms the above analysis and indicates that the $\tan\beta$ upper bounds are essentially inexistent.

This also illustrates that a “global” top-down fit, whatever elaborated with MINUIT algorithms, may be fooled and lead to misleading conclusions due to extra parameter dependence that originates from theoretical approximation artifacts (e.g. here the choice of EWSB scale, RGE approximation, etc). In the present case one could of course easily avoid such problems by simply adding protections within the minimization procedure, but that would amount to put explicitly the (model-dependent) upper bound on $\tan\beta$ due to tachyonic (or more generally too light) $\tilde{\tau}_1$.

We finally examine two questions related to theoretical uncertainties that are relevant to the above analysis. First, as already mentioned in deriving the $m_0^{q,l}$ constraints in Eqs. (22-23) we had neglected for simplicity the errors on s_W^2 : the latter are actually not quite negligible, since even a small uncertainty can in principle affect our determination from Eq. (17). However, the bulk of radiative correction contributions to the \bar{s}_W^2 parameter in the \overline{DR} scheme, originates from standard model and are thus predictable in our framework. Additional supersymmetric contributions are not negligible either[38], but we checked that varying all MSSM parameters and sparticle masses from the SPS1a to models with arbitrary MSSM values produces a variation of \bar{s}_W^2 of about 0.6% only. One may probably push parameters to extreme values to find a slightly larger variation, so we conservatively consider a 1% uncertainty on \bar{s}_W^2 . The impact on m_0 determination is an (upper) shift by about ~ 3 GeV with respect to the numbers quoted in Eqs. (22-23). Note that the correct dependence of m_0 and $\tan\beta$ upon \bar{s}_W^2 is automatically taken into account in the MINUIT fit results in Table 4.

Another potential question is that the determination of $m_0^{q,l}$ via Eq. (17) plus RGE, depends only on the cascade masses if restricting the RGE to one-loop order. At two-loop order, practically all other MSSM parameters are entering the RGE. Nevertheless, it is possible to study the impact of this uncertainty by assuming, within the two-loop RGE level, simple (e.g. universal) relations for the unknown parameters, and to redo our analysis: while central values are evidently shifted, the impact on error propagation is rather negligible, with minor quantitative changes on e.g. the obtained $m_0^{q,l}$ constraints. This is also consistent with some comparisons we made of two-loop versus one-loop RGE fit results using MINUIT.

We thus conclude that $\tan\beta$ is essentially unconstrained from the data we used at this stage, which is not much a surprise and consistent with general expectations on LHC prospects[5, 23]. Model-independent constraints on $\tan\beta$, though moderate, may be obtained however from other sectors as we shall see in next sections, either the sbottoms or the lightest Higgs mass measurements.

5 Third generation squark parameter determination

We consider now the third generation squarks. As discussed in section 2, sbottoms enter the gluino cascade and both mass eigenstates may be measured to some extent, though with less accuracy for the heaviest \tilde{b}_2 [5, 4]. We will examine what additional information they provide, both in unconstrained and constrained MSSM (with universality relation) as in previous sections.

5.1 Scenario S5: constraints from the sbottom masses in unconstrained MSSM

So far we got from the gluino cascade some useful information and constraint on the gaugino/Higgsino parameters, $m_0^{q,l}$ can be rather well determined, while $\tan \beta$ is very poorly constrained. The sbottom sector may provide information on the missing third generation soft scalar terms, or eventually on $\tan \beta$. To set up signs and other conventions let us recall the sbottom squared mass matrix:

$$M_b^2 = \begin{pmatrix} m_{Q3L}^2 + m_b^2 + (-\frac{1}{2} + \frac{1}{3}s_W^2)m_Z^2 \cos 2\beta & m_b(A_b - \mu \tan \beta) \\ m_b(A_b - \mu \tan \beta) & m_{bR}^2 + m_b^2 - \frac{1}{3}m_Z^2 \cos 2\beta \end{pmatrix} \quad (26)$$

where again all parameters are implicitly understood to be in the \overline{DR} scheme. It is clear that the trilinear term A_b will be very badly determined since it is very suppressed by the bottom mass m_b , with $\tilde{m}_b(Q_{EWSB}) \sim 3$ GeV in SPS1a. However, this also means that we can practically neglect A_b so that the sbottom masses determine, to a good approximation, the third generation parameters m_{Q3L}, m_{bR} in a simple way directly from (the trace of) (26):

$$m_{\tilde{b}_1}^2 + m_{\tilde{b}_2}^2 + \frac{m_Z^2}{2} \cos 2\beta - 2m_b^2 \equiv S = m_{Q3L}^2 + m_{bR}^2. \quad (27)$$

Now, taking one of the mass eigenvalue (say $m_{\tilde{b}_1}$) as a given function of the other parameters $\mu, \tan \beta$ etc, we can solve a simple relation for m_{Q3L}, m_{bR} :

$$m_{Q3L(bR)} = \left[\frac{S + (-)D}{2} \right]^{1/2} \\ D = -Y + \left[(m_{\tilde{b}_2}^2 - m_{\tilde{b}_1}^2 - 2m_b X_b)(m_{\tilde{b}_2}^2 - m_{\tilde{b}_1}^2 + 2m_b X_b) \right]^{1/2}, \quad (28)$$

where $Y = (-\frac{1}{2} + \frac{2}{3}s_W^2)m_Z^2 \cos 2\beta$ and $X_b = A_b - \mu \tan \beta$. There is in fact a twofold ambiguity, namely a second solution where $m_{Q3L} \leftrightarrow m_{bR}$ in Eq. (28), since it is a second order equation. For SPS1a we know that $m_{Q3L}(Q_{EWSB}) > m_{bR}(Q_{EWSB})$ resolves this ambiguity, but for a general MSSM one would have to deal in principle with the two possibilities. In addition one also expects radiative corrections to this tree-level determination which might spoil its simplicity. Radiative corrections to sbottom masses are not negligible in general, but to a very good approximation they are largely dominated by gluino and squark contributions, as already discussed in section 2.3. So

we have again a good control of these corrections, such that the running masses in the \overline{DR} scheme involved in Eqs (28) may be obtained from the pole masses after appropriate subtractions.

The resulting $m_{Q_{3L}}, m_{b_R}$ determination is illustrated in Fig. 13 where we plot the range of $m_{Q_{3L}}, m_{b_R}$ from a (uniform) scan over input mass accuracies from Table 1 and the other relevant parameters as indicated. Different situations are shown for a variation of $\tan\beta$ and μ within the previously obtained range, i.e. $\mu \sim 360 \pm 200$, or $\Delta\mu \pm 10$ (the latter values corresponding roughly to the case where three neutralino masses can be measured), and $3 \lesssim \tan\beta \lesssim 35$ (using the theoretical upper bound for SPS1a). Since A_b is essentially unknown at this stage, we vary it widely in the range $-1TeV - 1TeV$. As one can see the determination of $m_{Q_{3L}}, m_{b_R}$ is

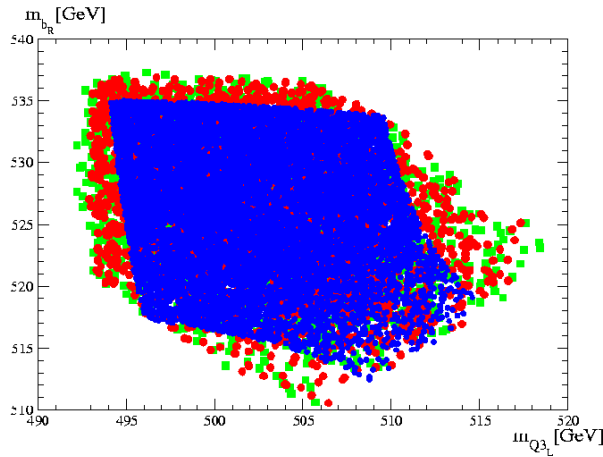


Figure 13: Constraints in general MSSM on $m_{Q_{3L}}, m_{b_R}$ from $m_{\tilde{b}_1}, m_{\tilde{b}_2}$ measurements in the gluino cascade decays. Radiative corrections from the pole to running masses have been subtracted out. Experimental errors on the sbottom masses are taken from Table 1. Blue region: fixed nominal values of $\tan\beta \sim 9.74, \mu \sim 357$ GeV (and $A_b = 0$). Red region: $3 \lesssim \tan\beta \lesssim 35, \Delta\mu \sim 10$ GeV, $-100GeV < A_b < 100GeV$; green region: $3 \lesssim \tan\beta \lesssim 50, \Delta\mu \sim 200$ GeV, $-1TeV < A_b < 1TeV$. Nominal SPS1a values are $m_{Q_{3L}} = 503$ GeV, $m_{b_R} = 525$ GeV (at one-loop RGE level).

quite accurate even in this general MSSM case and for largely unknown A_b . This is of course explained by the strong suppression of A_b which has thus practically no influence on the scalar mass parameter determination. Moreover, the variation of μ and even the large variation of $\tan\beta$ have no strong influence either, which is explained by the fact that they are both very suppressed also by m_b as compared to other parameters. To examine the impact of radiative corrections, we did a similar scan but neglecting on purpose the radiative corrections, i.e. using as central values the pole sbottom masses. As a result the $m_{Q_{3L}}, m_{b_R}$ central values are substantially shifted with respect to nominal SPS1a values, but the accuracy obtained on $m_{Q_{3L}}, m_{b_R}$ is very similar.

Next, in Fig. 14 we compare the previous results obtained from a simple scan with uniformly distributed random number with those from a scan made with Gaussian-distributed random num-

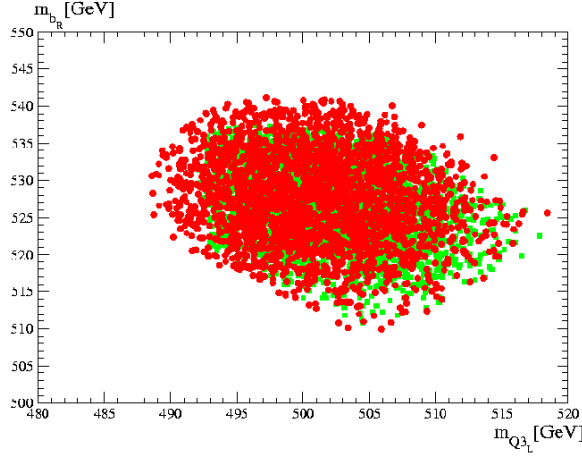


Figure 14: Comparison of uniform (in green) versus Gaussian (in red) scan with one- σ (68% C.L.) level contours. The variation of extra parameters correspond to the less determined range in Fig. 13, i.e.: $3 \lesssim \tan \beta \lesssim 50$, $\Delta\mu \sim 200$ GeV, $-1\text{TeV} < A_b < 1\text{TeV}$.

bers, defining a χ^2 domain similarly to the analysis in section 4. One can see that the corresponding one- σ limits show the expected statistical behaviour, having a more regularly-shaped contour than the one in the uniform case, but with no drastic changes in the limits on $m_{Q_{3L}}$, m_{b_R} .

5.2 Scenario S'_5 : constraints from sbottoms in MSSM with universality

Prospects for the third generation scalar terms are better in a constrained MSSM with universality relations in the scalar sector. In this case, one has:

$$m_0^{q,l} \equiv m_{Q_{3L}}(Q_{GUT}) = m_{b_R}(Q_{GUT}) \quad (29)$$

Next using the results from section 4 on $m_0^{q,l}$ limits and from a top-down RGE one can determine the corresponding accuracy obtained on $m_{Q_{3L}}(Q_{EWSB})$ and $m_{b_R}(Q_{EWSB})$:

$$m_{Q_{3L}}(Q_{EWSB}) \sim 498 \pm 1.2 \pm 7\text{GeV}, \quad m_{b_R}(Q_{EWSB}) \sim 521 \pm 1.8 \pm 6\text{GeV}, \quad (30)$$

where the first errors correspond to a variation of m_0 for fixed M_3 , while the second additional errors take into account the $m_{\tilde{g}} \sim M_3$ uncertainty, which dominates the final uncertainties. Alternatively, one may use here the limits on m_0 as obtained from the χ^2 minimization in Table 4, which would give results roughly comparable to the bounds in Eq. (30) (except that it is somewhat more difficult to disentangle the effect of M_3 uncertainties from the fit). Comparing with the general MSSM determination from the sbottom masses in Figs. 13,14 one can see a definite improvement on $m_{Q_{3L}}(Q_{EWSB})$ and $m_{b_R}(Q_{EWSB})$ accuracies by about a factor two. This may be sufficient to resolve the twofold ambiguity between $m_{Q_{3L}}$ and m_{b_R} in the above unconstrained MSSM.

Perhaps more interestingly one may expect to derive an independent determination of $\tan \beta$ in this universality case, by combining all information from m_0 and the sbottom masses. More

precisely, turning the other way round Eqs. (28) one can determine very simply $X_b = Ab - \mu \tan \beta$ in terms of the know parameters as follows:

$$2 m_b X_b = - \left[(m_{\tilde{b}_2}^2 - m_{\tilde{b}_1}^2)^2 - (m_{\tilde{Q}_{3L}}^2 - m_{\tilde{b}_R}^2 + Y)^2 \right]^{1/2}. \quad (31)$$

(Actually Eq. (31) comes from a second order equation so strictly speaking there is again a twofold ambiguity: $m_b X_b = \pm [\dots]^{1/2}$, but within our sign convention, if $\mu > 0$ $X_b < 0$ necessarily, even for general MSSM, unless $|\mu| \tan \beta < A_b$ which is not a very common situation except perhaps for very small $\tan \beta$ values.)¹¹

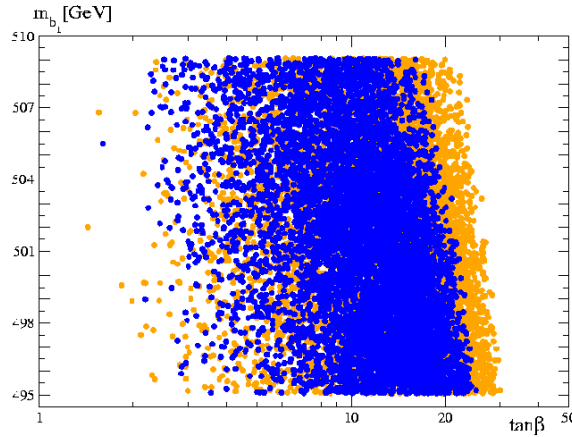


Figure 15: Constraints on $\tan \beta$ with uniform scan from $m_{\tilde{b}_1}, m_{\tilde{b}_2}$ accuracies. A_b practically undetermined ($A_b = A_b(\text{SPS1a}) \pm 1 \text{ TeV}$). In blue : $\Delta m_{\tilde{b}_2} = 7.9 \text{ GeV}$. In orange: $\Delta m_{\tilde{b}_2} = 16 \text{ GeV}$.

The resulting determination of X_b and $\tan \beta$ from Eq. (31) is first illustrated in Fig. 15: while X_b is directly determined from Eq. (31), for $\tan \beta$ one has to take into account the additional uncertainties in the determination of μ , and A_b which is assumed to be essentially unknown at this stage. However it is clear that this has a moderate impact on $\tan \beta$ determination, since even a large variation $-1 \text{ TeV} < A_b < 1 \text{ TeV}$ has a moderate effect $\sim \Delta A_b / \mu$ (unless if $|\mu|$ would be very small). So even at this stage where A_b is completely undetermined, reasonable constraints on $\tan \beta \lesssim 27 - 28$ are obtained, as shown by the blue contour. Moreover even when increasing the $m_{\tilde{b}_2}$ uncertainty by a factor of two, i.e. $\Delta m_{\tilde{b}_2} \sim 16 \text{ GeV}$, it remains some reasonable constraints on $\tan \beta \lesssim 30$, see Fig. 15 (though we note that any constraints on $\tan \beta$ disappear if the \tilde{b}_2 is not measured at all). Like for the previous section analysis we also show the difference between uniform and Gaussian scans, with corresponding one- and two- σ contours in Fig. 16. For completeness the joint correlated determination of $(\tan \beta, X_b)$ is also shown in Fig. 17.

We thus observe that, provided the two sbottom masses can be measured with this accuracy at LHC, the bounds on $\tan \beta$ may start to be rather interesting, at least at the one- σ level. These

¹¹Note also that $\tan \beta$ enters both sides of Eq. (31) via the D-term $Y = (-\frac{1}{2} + \frac{2}{3}s_W^2)m_Z^2 \cos 2\beta$ so that one has to iterate on $\tan \beta$, but this iteration is converging fastly.

results are also confirmed by a χ^2 minimization fit using MINUIT, with more or less comparable bounds obtained, as shown in Table 5. We finally mention that squark and slepton universality

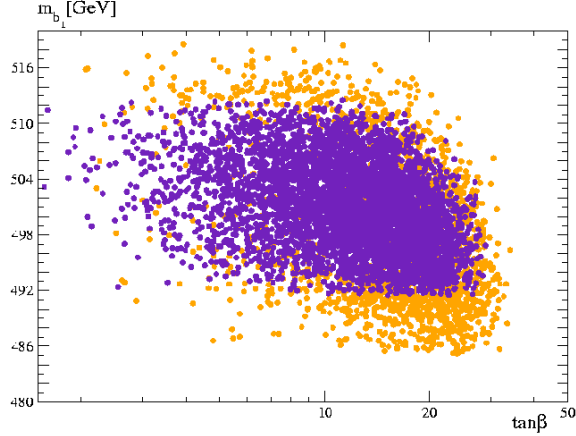


Figure 16: Constraints on $\tan \beta$ from Gaussian scan: indigo: one- σ (68% C.L.); in orange: two- σ (95% C.L.).

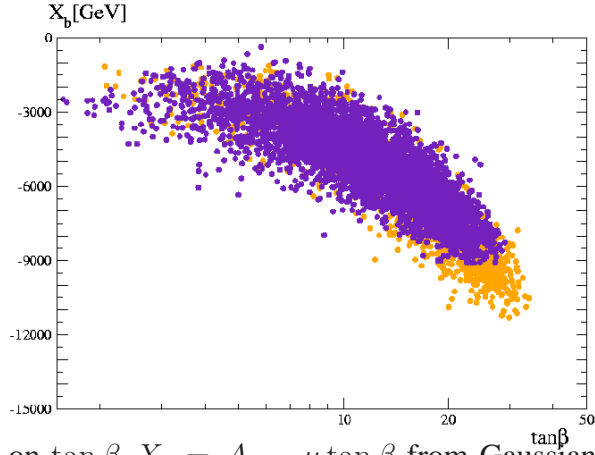


Figure 17: Constraints on $\tan \beta$, $X_b = A_b - \mu \tan \beta$ from Gaussian scan: indigo: one- σ (68% C.L.); orange: two- σ (95% C.L.).

relations as in Eq. (29) is yet not enough to have any interesting determination of A_b , which is quite obvious from its very suppressed contributions to the mass matrix (26). One thus needs a different strategy to determine, if possible, the remaining trilinear couplings. The prospects for the latter would be certainly much better if one could measure the stop masses in such cascades. This is not the case for the SPS1a, but we will examine in the next section how the Higgs sector parameters can help to determine the stop sector trilinear couplings.

Table 5: Constraints on $m_0, \tan \beta$ obtained from a standard top-down χ^2 fit of squark +sbottom masses and neutralino/gluino masses for different level of MINUIT minimizations.

Data & fitted parameter (+ model assumptions)	MIGRAD minimization (68%C.L.)	MINOS minimization (68%C.L.)	nominal SPS1a value
$m_{\tilde{e}_2}, m_{\tilde{u}_1}, m_{\tilde{b}_{1,2}} +$ $m_{\tilde{N}_1}, m_{\tilde{N}_2}, m_{\tilde{g}}$ (1-loop RGE + no \tilde{q} R.C)	(convergent)	$\tan \beta$ exceed limits	
$m_0^{q,l}$	99.96 ± 9.9	$99.9^{+10}_{-10.4}$	100
$m_{1/2}$	250 ± 3.6	250 ± 3.6	250
$\tan \beta(m_Z)$	9.98 ± 13.6	$9.98^{+13.6}_{-\text{no limits}}$	10

6 Bottom-up reconstruction of Higgs sector parameters

In the Higgs sector, the most relevant parameters (at tree-level) are the scalar mass terms m_{H_u}, m_{H_d} and $\tan \beta$. These may be replaced equivalently, using the EWSB conditions, by μ , the pseudoscalar mass m_A , and $\tan \beta$. More precisely, the EWSB minimization equations $\partial V_{\text{Higgs}}/\partial H_d = 0$; $\partial V_{\text{Higgs}}/\partial H_u = 0$ (where V_{Higgs} designates the MSSM scalar potential) can be solved for μ^2 and $B\mu$:

$$\begin{aligned}\mu^2 &= \frac{1}{2} [\tan 2\beta (m_{H_u}^2 \tan \beta - m_{H_d}^2 \cot \beta) - m_Z^2] \\ B\mu &= \frac{1}{2} \sin 2\beta [m_{H_u}^2 + m_{H_d}^2 + 2\mu^2]\end{aligned}\quad (32)$$

which eventually includes radiative corrections to the scalar potential in the form of tadpole corrections t_u, t_d [49, 38]:

$$m_{H_u}^2 \rightarrow m_{H_u}^2 - t_u/v_u \text{ and } m_{H_d}^2 \rightarrow m_{H_d}^2 - t_d/v_d \quad (33)$$

while the running $m_A(Q)$ is defined as:

$$\bar{m}_A^2(Q) = m_{H_d}^2(Q) + m_{H_u}^2(Q) + 2\mu^2(Q) \quad (34)$$

(where as previously all parameters are implicitly understood to be in the \overline{DR} scheme). The A pole mass is then related to $m_A(Q)$ via additional radiative corrections[40, 38]. It is well-known, however, that in the MSSM the scalar top sector contributes largely to radiative corrections to m_h and m_A . Thus even if some parameters are available from other sector analysis (though not precisely for $\tan \beta$), only an independent measurement of m_A (or alternatively an information on the stop sector, on $X_t \equiv A_t - \mu/\tan \beta$) could give a more useful information on the remaining parameters. For the determination of these Higgs parameter sector in a general MSSM case, the

prospects are thus not very good if the available data are similar to those of the SPS1a benchmark, even if the lightest Higgs mass m_h could be determined with a good accuracy. In a constrained MSSM with complete high scale universality of scalar soft terms, prospects are possibly better. We can then use our previous analysis with in addition:

$$m_0^{q,l} \equiv m_{H_u}(Q_{GUT}) = m_{H_d}(Q_{GUT}) \quad (35)$$

to determine μ via Eqs. (32) as well as the running m_A value in Eq. (34). From Eq. (32) one has very roughly for $\tan \beta \gg 1$: $\mu^2 \sim -m_{H_u}^2$ which is largely insensitive to $\tan \beta$. (NB in our analysis we use of course the complete expressions from Eqs. (32)). Thus the rather good determination of m_0 from the squark and slepton sector, as analyzed in previous section, together with universality assumptions (35) give a more precise determination of $\mu(Q_{EWSB})$. However, m_{H_u} has a strong sensitivity to the trilinear stop coupling A_t through its RGE via terms $\propto y_t^2 A_t^2$, that restricts a very good determination of μ . Typically for $4 \lesssim \tan \beta \lesssim 50$ and very moderate variation of A_t , $\Delta A_t \sim 100$ GeV, we obtain:

$$330 \text{ GeV} \lesssim \mu(Q_{EWSB}) \lesssim 360 \text{ GeV} \quad (36)$$

being comparable to the accuracy obtained in a general MSSM from neutralino mass measurements when a third neutralino can be measured, see section 3.3. Now for less limited $\Delta A_t \sim 200$ GeV (which corresponds approximately to the range of variation we obtain once using all input, as we shall see) those bounds are somewhat increased:

$$300 \text{ GeV} \lesssim \mu(Q_{EWSB}) \lesssim 410 \text{ GeV} \quad (37)$$

Note these bounds are very insensitive to m_0 values within its accuracy determined by squarks and sleptons in section 4. The limits (36), (37) are to be compared with the less model-dependent constraints on μ obtained solely from the neutralino/gluino sector in section 3.

6.1 Naive tree-level counting of parameters

Let us first start with simple tree-level analysis in order to delineate the parameters entering in game. Concerning the lightest scalar Higgs mass, at tree-level, $m_h^{2,tree}$ is given by:

$$m_h^{2,tree} = \frac{1}{2} \left[m_A^2 + m_Z^2 - ((m_A^2 + m_Z^2)^2 - 4m_A^2 m_Z^2 \cos^2 2\beta)^{1/2} \right] \quad (38)$$

Inverting these relations gives a (unique) solution for m_A :

$$\bar{m}_A^2 = \frac{\bar{m}_h^2(m_Z^2 - \bar{m}_h^2)}{m_Z^2 \cos^2 2\beta - \bar{m}_h^2} \quad (39)$$

from which one also derives:

$$m_{H_u}^2 = \frac{\bar{m}_A^2 - (\mu^2 + m_Z^2/2)(\tan^2 \beta - 1)}{\tan^2 \beta + 1}, \quad m_{H_d}^2 = m_A^2 - m_{H_u}^2 - 2\mu^2. \quad (40)$$

So very naively one may have thought to equate Eqs. (34) with Eq. (39), deriving from this precise $\tan \beta$ constraints typically. But, as already mentioned, this tree-level analysis would be very unrealistic since the lightest Higgs mass m_h and m_A get large radiative corrections already at one-loop level mainly from the stop loops, that are enhanced by a m_t^4 dependence. Rather, as we did for the other sectors we will try to incorporate these large corrections consistently.

6.2 Reconstruction of Higgs sector parameters in constrained MSSM

The MSSM neutral Higgs squared-mass matrix reads, including radiative corrections:

$$\begin{pmatrix} m_Z^2 \cos^2 \beta + m_A^2 \sin^2 \beta + S_{11} & -(m_Z^2 + m_A^2) \sin \beta \cos \beta + S_{12} \\ -(m_Z^2 + m_A^2) \sin \beta \cos \beta + S_{12} & m_Z^2 \sin^2 \beta + m_A^2 \cos^2 \beta + S_{22} \end{pmatrix} \quad (41)$$

where S_{ij} designate generically loop self-energy contributions. To simplify the procedure let us first write a very simple approximation for m_h (see e.g. [50]):

$$m_h^2 = m_h^{2,tree} + \frac{3g_2^2 m_t^4}{8\pi^2 m_W^2} \left[\ln \left(\frac{m_{\tilde{t}_1} m_{\tilde{t}_2}}{m_t^2} \right) + \frac{X_t^2}{M_S^2} - \frac{X_t^4}{12M_S^4} \right] \quad (42)$$

where

$$\begin{aligned} X_t &= A_t - \mu \cot \beta \\ M_S^2 &= [m_Q^2 m_{t_R}^2 + m_t^2 (m_Q^2 + m_{t_R}^2) + m_t^4]^{\frac{1}{2}} \\ m_{\tilde{t}_1} m_{\tilde{t}_2} &= [M_S^4 - 4m_t^2 X_t^2]^{\frac{1}{2}} \end{aligned} \quad (43)$$

(and g_2 is the $SU(2)$ gauge coupling). There is a large literature on various approximations to the m_h mass radiative corrections. We emphasize that in our actual analysis we do not use the simple Eq. (42) but a more elaborated expression, yet giving compact expressions for the needed S_{ij} in Eq. (41)[39]. (This compact approximation is included in SuSpect as one possible Higgs mass calculation option). The latter incorporates some of the leading two-loop effects, but depends only on the very same parameters as in Eq. (42) (apart from SM-like parameters).

At this stage, if a rather precise information on the stop sector would be available we could use an improved version of Eq. (39), incorporating radiative corrections¹², to derive m_A independently from the relation (34). However within the SPS1a input assumptions this would not give any useful constraints (given also the poorly known $\tan \beta$ constraints). We thus rather assume universality relation (35) so that Eq. (34) together with the m_h measurement can determine both X_t and $\tan \beta$. Since we also assume complete universality of the squark sector, we can use the previous m_0 determination to calculate also the stop sector soft terms $m_{\tilde{t}_R}$ and $m_{\tilde{Q}_{3L}}$ (the latter already obtained from the sbottom sector), as needed in Eq. (42) or its more complete generalization [39] actually used in the numerics below. The simplified expression of m_h we used is remarkably close

¹²Note that even the full one- (two)-loop Higgs radiative corrections, i.e. with full expressions of the S_{ij} above, do preserve a *linear* m_A^2 solution in terms of m_h similarly to Eq. (39) but with appropriate corrections from S_{ij} .

to the full one-loop (plus leading two-loop) values[38, 51, 40] (in the \overline{DR} scheme), with at most a 2 GeV discrepancy (and often much less) for a large range of MSSM parameters. For the relevant SPS1a case we find $m_h^{simp} = 111.28$ GeV, while $m_h^{2-loop} = 110.90$ GeV.

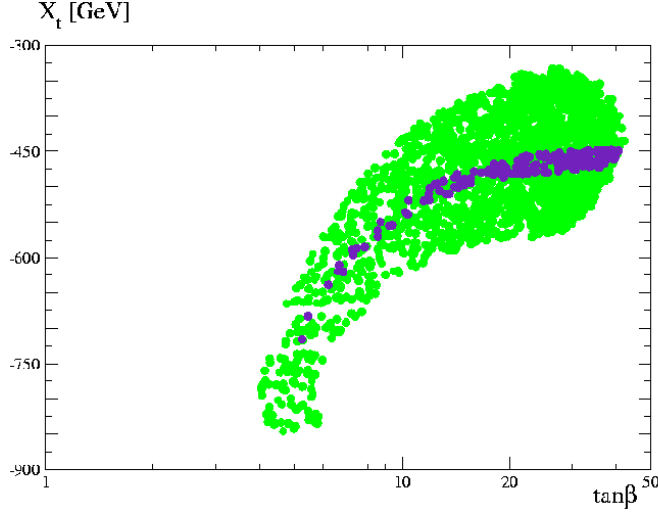


Figure 18: Constraints on $\tan \beta$ and $X_t \equiv A_t - \mu/\tan \beta$: indigo: one- σ (68% C.L.) from a gaussian scan; green: same contour but for theoretical uncertainties $\Delta m_h = 2$ GeV instead.

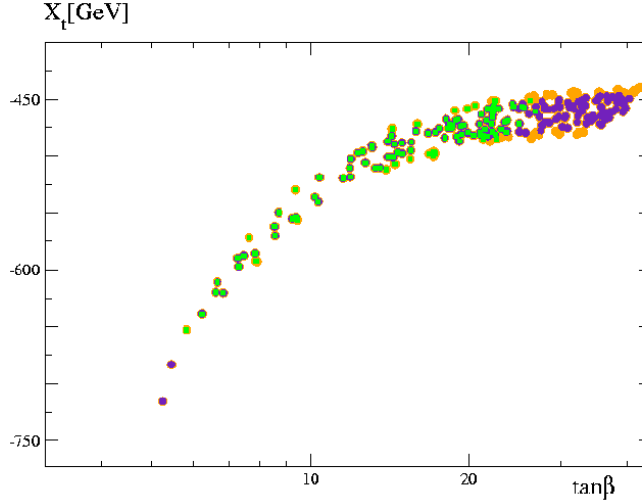


Figure 19: Constraints on $\tan \beta$ and $X_t \equiv A_t - \mu \tan \beta$: indigo: one- σ (68% C.L.); orange: additional points at two- σ (95% C.L.); green squares: remaining points (one- σ level) when adding sbottom mass measurements.

We thus perform scan over parameters, taking into account the previous constraints on m_0 from squark and slepton sector (and letting X_t arbitrary), deriving resulting joint constraints on $X_t, \tan \beta$. The variation of other parameters that is implied (like the variation of μ from EWSB relations (32) is consistently taken into account. This is illustrated first in Fig. 18, where the

range of points obtained from the experimental prospect $\Delta m_h(\text{exp}) \sim 0.25$ from Table 1, are shown, as well as those corresponding to theoretical uncertainties in the Higgs mass calculations (we take the latter as $\Delta m_h(\text{th}) \sim 2 \text{ GeV}$ [40, 47]). Note again that the density of points in the $\tan \beta, X_t$ plane has no precise statistical meaning: the concentration seen for rather large $\tan \beta$ is an artifact of the logarithmic scale, while the one- σ band being thinner for low $\tan \beta$ and small X_t , is easily explained from the m_h dependence on $\tan \beta$ and X_t : more precisely for fixed $\tan \beta$, $m_h(X_t)$ reaches a maximum for a certain X_t (see e.g. [40]), and it is more difficult to match the approximate SPS1a value of m_h for both small $\tan \beta$ and large (negative) A_0 . The range of $\tan \beta$ as obtained from this experimental Higgs mass measurement, at the one- σ level, is thus approximately determined as:

$$5 \lesssim \tan \beta \lesssim 40 \quad (44)$$

These bounds are strongly correlated with X_t values, as the figure shows. For X_t one finds approximately:

$$-730 \text{ GeV} \lesssim X_t \lesssim -450 \text{ GeV} \quad (45)$$

Note also that all points shown with relatively large $\tan \beta \sim 35 - 40$ are passing the previously mentioned theoretical constraint of no tachyon $\tilde{\tau}_1$, since when departing from the true SPS1a benchmark, larger values of $\tan \beta$ can be compensated by values of $A_0 > -100 \text{ GeV}$. (This is of course not taking into account any additional experimental constraints on $m_h, m_{\tilde{\tau}}$, etc which, as already emphasized, are omitted here since they are more model-dependent constraints.) The resulting limits on X_t and $\tan \beta$ are of course sensitive to m_h theoretical uncertainties as shown on the figures (though very little as concerns the $\tan \beta$ upper bound). In this case we obtain:

$$4 \lesssim \tan \beta \lesssim 40; \quad -850 \text{ GeV} \lesssim X_t \lesssim -330 \text{ GeV} \quad (46)$$

However the contours shown in Fig. 18 did not take into account yet the additional constraints from the sbottom mass measurements as were obtained in previous section 5. This is added in Fig. 19 (in green), where the one and two- σ domains obtained from m_h measurement are compared. One can see that at the two- σ level the X_t range increases slightly, for large $\tan \beta$, while the $\tan \beta$ bounds are not much affected. On the other hand, the sbottom mass constraints put further upper limits on $\tan \beta \lesssim 27 - 28$, in consistency with the previous analysis in section 5.

These results are also compared with a top-down MINUIT minimization in Table 6, using as input data m_h together with the gluino cascade sparticles (but not yet using the sbottom masses at this stage). One observes that the MIGRAD symmetric error on $\tan \beta$ appears to be very good, but comparing with the contours in Figs. 18,19 one can suspect that it is essentially influenced by the *lowest* limit on $\tan \beta$, and that the actual errors are particularly unsymmetrical due to the flat behaviour for large $\tan \beta$. This seems confirmed by the fact that the unsymmetrical MINOS positive error is not calculated by MINUIT. The lower $\tan \beta$ bound on the other hand is very consistent with our alternative finding in Eq. (44). This behaviour is well explained by the flattest dependence for large $\tan \beta$ as clearly illustrated by the plots in Figs. 18,19. For completeness we also show in Fig. 20 the corresponding one- and two- σ domains but in the $(\tan \beta, A_0)$ plane, with

Table 6: Constraints on mSUGRA parameters $m_0, m_{1/2}, A_0, \tan \beta$ obtained from a standard top-down χ^2 fit of (first two generation) squark, sleptons, neutralino/gluino masses, plus the lightest Higgs mass, for different level of MINUIT minimizations.

Data & fitted parameter (+ model assumptions)	MIGRAD minimization (68%C.L.)	MINOS minimization (68%C.L.)	nominal SPS1a value
$m_{\tilde{e}_2}, m_{\tilde{u}_1}, +$ $m_{\tilde{N}_1}, m_{\tilde{N}_2}, m_{\tilde{g}} + m_h$ (1-loop RGE + no \tilde{q} R.C)	(convergent)	(problems)	
$m_0^{q,l}$	99.96 ± 11.8	$99.9^{+11.5}_{-10}$	100
$m_{1/2}$	250 ± 4.9	250 ± 4.9	250
A_0	-100.5 ± 150.0		-100
$\tan \beta(m_Z)$	9.97 ± 4.3	$9.97^{+no}_{-4.3} \text{ limits}$	10

the range corresponding to adding sbottom mass measurements. One can see that the sbottom mass bound have some impact on A_0 bounds, at least for large $-A_0$. These results may be compared with the A_0 limits obtained from the MINUIT fit in Table 6.

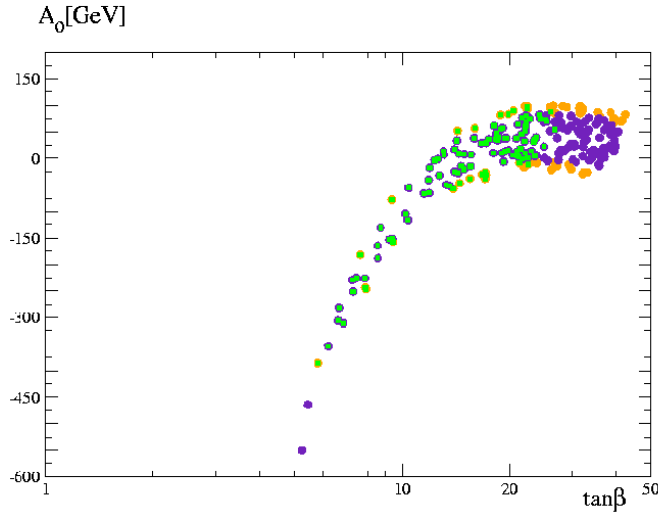


Figure 20: Contours in the plane $(\tan \beta, A_0)$: indigo: one- σ (68% C.L.) from a gaussian scan; orange: two- σ (95% C.L.) from a gaussian scan.

Thus the m_h measurement alone gives a mild upper bound on $\tan \beta$ in the case where only some knowledge on $m_A(Q_{EWSB})$ is assumed but not on X_t . The improvement on $\tan \beta$ limits is mainly coming from adding the sbottom mass measurements. However this mild sensitivity as well as the strong $\tan \beta - X_t$ correlation is essentially determined by the variation of A_0 which

is assumed unknown at this stage. The uncertainties on μ (that are reasonable in this constrained MSSM case) have little influence (except perhaps for very small $\tan\beta$), since it is suppressed as $\mu/\tan\beta$ within X_t . We shall see in the summarizing section 6.3 that overall the bounds are a bit tighter once combining all available information, except those for A_0 which depend quite much on the level of approximation used in RGE and radiative corrections. If an additional independent information on A_0 would be available (e.g. if the stop masses could be measured) the constraints in the $\tan\beta, X_t$ plane could be evidently improved. Clearly also better constraints on $\tan\beta$ are prospected[5] if some of the heavy Higgses A, H, H^\pm could be measured, that we do not assume in our ‘minimal’ set of input mass measurements and within the SPS1a benchmark. (It would be rather straightforward, however, to extend our above analysis in case such additional information would be available.)

We finally mention that our results are not drastically changing once using the more complete two-loop level radiative corrections for m_h (assuming in such case universality/mSUGRA relations to calculate all higher order corrections), except for the bounds on A_0 that are substantially worsening in this case, as will be confirmed by further MINUIT fit results summarized in section 6.3. This is easily explained from the flattest dependence of $m_h(A_0)$ for large $-A_0$ at the two-loop level, in the considered range of the other relevant parameters. As far as we can see, this may be explained by the fact that within the two-loop level radiative corrections to m_h [40, 51] there is somewhat much room for possible cancellations of the A_0 dependence entering in higher orders, most notably in all squark and stau contributions both at the one- and two-loop level. This is another example of the caution to interpret results when performing minimization constraints using different level of theoretical approximations.

6.3 Combining all information and comparison with standard fits

We finally summarize and combine all previous constraints from the different sectors, both in general MSSM or with universality relations in Table 7. By “combined best constraints” we mean simply evaluating the joint limits by crudely superposing the constraints obtained in the three different sectors of gaugino/Higgsino, squarks/sleptons and Higgs, which eventually results in slight improvements on some parameter limits. We did not attempt to perform a more elaborated statistical combination of the three sector constraints within our approach. However these results are compared with those obtained from a top-down χ^2 fit of basic mSUGRA parameters to the same mass measurements in Table 8. As one can see the results are overall qualitatively consistent, except perhaps for the A_0 limits. The fact that A_0 bounds (and to some extent $\tan\beta$ bounds as well) are worsen when fitting parameters in mSUGRA at the full two-loop level instead of one-loop was explained previously due to the possible cancellations of the A_0 dependence in higher order m_h contributions. Note that for $\tan\beta$, the MIGRAD symmetric minimization error found here appears very optimistic as compared to the upper bound derived from the bottom-up reconstruction, $\tan\beta \lesssim 28$. As already mentioned above it is possibly much influenced by the *lower* bound that results from the combination with the Higgs sector measurements. The MINOS upper bound is

Table 7: Combined best constraints from all gluino cascade decay sparticles and lightest Higgs mass measurements for the bottom-up approach in different MSSM scenarios.

Model or assumptions	Parameter	Constraint (GeV)	nominal SPS1a value (from SuSpect 2.41)
general MSSM	$M_1(Q_{EWSB})$	$\sim 95\text{--}115$	101.5
” ”	$M_2(Q_{EWSB})$	$\sim 175\text{--}220$	191.6
” ”	$M_3(Q_{EWSB})$	$\sim 580\text{--}595$	586.6
” ”	$(\frac{3}{8}m_{uL}^2 + \frac{m_{eR}^2}{4})^{1/2}(Q_{GUT})$	$\sim 68\text{--}89$	$(\frac{5}{8})^{1/2}100 \sim 79$
” ”	$m_{Q3L}(Q_{EWSB})$	$\sim 488\text{--}518$	497
” ”	$m_{bR}(Q_{EWSB})$	$\sim 510\text{--}540$	522
” ”	$\mu(Q_{EWSB})$	$\sim 280\text{--}750$	357
” ”	$\tan \beta(Q_{EWSB})$	$\sim 1\text{--}36$ (th. bounds)	9.74
+ m_{N_4}	$\mu(Q_{EWSB})$	$\sim 350\text{--}372$	357
” ”	$\tan \beta(Q_{EWSB})$	$\sim 2.7\text{--}36$ (th. bounds)	9.74
\tilde{q}, \tilde{l} -universality	$m_0^{q,l}(Q_{GUT})$	$\sim 90\text{--}112$	100
” ”	$m_{Q3L}(Q_{EWSB})$	$\sim 490\text{--}506$	497
” ”	$m_{bR}(Q_{EWSB})$	$\sim 513\text{--}530$	522
$M_i, i = 1, \dots 3$ -universality	$M_i(Q_{GUT})$	$\sim 245\text{--}255$	250
\tilde{b}_1, \tilde{b}_2 -universality	$\tan \beta(Q_{EWSB})$	$\sim 3\text{--}28$	100
mSUGRA	m_0	$\sim 90\text{--}112$	100
	$m_{1/2}$	$\sim 245\text{--}255$	250
	$-X_t$	$\sim 450\text{--}730$	530
	$-A_0$	$\sim -100\text{--}350$	100
	$\tan \beta(m_Z)$	$\sim 5.5\text{--}28$	10

however more consistent with the bottom-up result.

Table 8: Combined constraints on mSUGRA basic parameters from a standard top-down χ^2 fit with MINUIT of all gluino cascade decay sparticle masses plus m_h measurements.

Model and assumptions	Parameter	68% C.L. limits (GeV)	SPS1a value
mSUGRA	m_0	99.96 ± 11.2	100
2-loop RGE + full \tilde{q} R.C. + 2-loop m_h		(99.95 ± 11.7)	
(1-loop RGE+ no \tilde{q} R.C. +simple m_h R.C.)	$m_{1/2}$	250.0 ± 3.7	250
		(249.5 ± 4.7)	
	A_0	-104.2 ± 379	-100
		(-100.6 ± 136)	
	$\tan \beta(m_Z)$	$9.9^{+9.4}_{-4.7}$	10
		(9.96 ± 4.11)	

7 Conclusion

We have examined some specific bottom-up reconstruction strategies at the LHC for general and universality-constrained MSSM parameters, starting from a plausible set of incomplete measurements of few MSSM sparticles. Using mass measurements mainly from cascade decays of gluino and squarks, and the lightest Higgs boson mass, we have constructed different algorithms based on rather simple semi-analytical inverse relations between the MSSM basic parameters and mass spectrum, incorporating radiative corrections at a realistic level. We have determined constraints on the relevant basic MSSM parameters from the expected mass accuracies, under different theoretical assumptions on the degree of universality of some of the parameters. These constraints have been also compared at different stages of a sector-by-sector analysis with those obtained from more conventional top-down approaches with minimization fits of data. The results are overall consistent, which is an a posteriori check that our rather naive semi-analytic approach with many approximations does essentially capture the sensitivity on parameters.

Regarding the SPS1a reconstruction example studied here, more quantitatively we have shown that a rather limited data set, consisting of merely the measurement of sparticle masses involved in gluino cascade decay to a few percent accuracy, may still provide reasonably good constraints on some of the relevant MSSM parameters. This is in particular the case for the gaugino mass parameters and the squark and slepton soft mass terms, even for unconstrained MSSM without universality assumptions. If a precise measurement of the lightest Higgs mass is available, additional constraints (though moderate) on $\tan\beta$, $X_t \equiv A_t - \mu/\tan\beta$ are obtained but only under Higgs-sfermion mass term universality assumptions. Interesting constraints for a general MSSM are however more challenging to obtain in general for the Higgs sector parameters (as well as for $\tan\beta$), unless more precise measurements would be available (or data from another sector like heavy Higgses and/or scalar top masses typically), as is also known from other analysis[5]. We stress again that considering only the gluino/squark cascade (plus the lightest Higgs) sparticle identification in our analysis is not motivated by a strong prejudice against other potential SUSY-discovery processes at the LHC. Indeed the cascade in Eq. (1) may be considered already quite specific from a general MSSM viewpoint, but it gives us a well-defined “minimal” input set for testing our approach and comparing it with other analysis for the very much studied SPS1a benchmark. Even if our results are probably not very new to the experts, they illustrate that a step-by-step semi-analytic approach can help to better exhibit the sensitivity of specific MSSM parameter to given sparticle mass or other data, that may be more difficult to grasp from global top-down fits. In some cases the non-linear and non-symmetric behaviour of error propagations is exhibited by the bottom-up approach in a more explicit way (as illustrated typically here for $\tan\beta$, comparing Tables 7 and 8). As compared to other recent analysis of MSSM constraints at LHC from similar data (e.g. [5, 17, 8, 25]), our results cannot be compared quantitatively in very detail since the data used are often different (with generally more input sparticle masses fitted in most other analysis). We find however a rough consistency on the expected sensitivity of the basic

MSSM parameters, as above discussed.

The relatively simple algorithms described here are rather flexible and may be easily interfaced with more elaborated simulation tools, that would allow in particular a more realistic statistical treatment of the different sources of data and theoretical uncertainties. Also some analytical relations may also be used at least as “Bayesian priors” guideline to other analysis, in a way complementary to the Markov chain techniques. We plan indeed a more refined statistical analysis in the future[41], by possibly combining our approach with Bayesian and Markov chain techniques of ref. [8, 25, 17].

Our approach may thus provide a useful complementarity to more elaborated simulations as well as possible cross-checks. Moreover it is not at all restricted to the LHC phenomenology: some of the algorithms described here, for instance in the neutralino and squark/slepton sectors, may be readily used for ILC data upon straightforward changes in sparticle mass accuracies. However, a similar approach for the ILC, following for instance works in refs. [20, 24], deserves specific analysis beyond the scope of the present paper due to the different sparticle spectrum expected to be reached at the ILC, that will imply slightly different inversion algorithms.

Acknowledgements

This work is partially supported by ANR contract “PHYS@COL&COS” and GDR 2305 “Supersymétrie”. We are grateful to Gilbert Moulhaka for stimulating conversations at a preliminary stage of this work. We also thank Dirk Zerwas, Ulrich Ellwanger and Sabine Kraml for interesting comments or discussions.

A Bottom-up renormalization group evolution in SuSpect code

In this section we illustrate in some details an important ingredient of our bottom-up reconstruction procedure which is the renormalization group evolution (RGE)[26, 27] of MSSM parameters from low to high energy. We take this opportunity to present the results from an available option of the SuSpect code, illustrating some properties of this bottom-up RG evolution which are quite general and independent of the present analysis and LHC cascade decay phenomenology. (This option has recently been adapted to the more suitable “Les Houches accord” input file conventions[52].)

The fact that the RGE for the MSSM parameters are “invertible”, i.e. can be evolved from high to low scale and backward, is a rather obvious feature of any such coupled differential equations. However, what makes it less straightforward in the standard approach to MSSM calculation with RGE is that there are actually three (at least) different energy scales in the game, with corresponding boundary conditions:

- the high (generally GUT) scale, at which one defines e.g. the mSUGRA parameters with eventually some universality relations;
- the (low) electroweak symmetry breaking scale, at which the soft breaking and other relevant MSSM parameters are evolved to in a standard top-down evolution;
- finally the scale m_Z , or eventually some other low energy scale, which enter as other boundary conditions e.g; via the precise measurements of the gauge couplings.

The interplay between these different scales in MSSM spectrum calculation codes (such as SuSpect [31] and similar codes[28, 29, 30]) needs among other things iterative algorithms for the evolution between the three different scale with a consistent implementation of any possibly known radiative corrections to the parameters (gauge couplings, top, bottom masses, etc) entering as boundary conditions to the RG evolution. (We refer to the SuSpect manual [31] for details on such RGE algorithms.)

Such a bottom-up evolution option has been available in a beta-version for some time in SuSpect but was not publicly available nor illustrated until now. In Table 9 we illustrate for the SPS1a benchmark point this bottom-up RG evolution of all parameters. We show in particular some important features on the error propagation in such a procedure, and which parameters are more sensitive to this dispersion. The input parameters (in the second column) were obtained in a first stage from a standard (top-down) run from the mSUGRA SPS1a input parameters in Eq. (2) (with $m_{top} = 175$ GeV). The third column gives the corresponding output values resulting from a RG evolution up to a GUT scale from a bottom-up SuSpect run under the most general MSSM assumptions, i.e. without any a priori on possible universality relations at the GUT scale. One can already notice from this that the agreement with the original mSUGRA parameter values is excellent: the discrepancies are of order $\mathcal{O}(10^{-3})$ that are in fact consistent with the accuracy chosen (i.e. the intrinsic error of the numerical evolution of the RGE as performed with a Runge-Kutta algorithm, as well as the intrinsic error due to necessary iterative procedures[31]). We point out

however that the results shown here correspond to the choice of m_{H_u}, m_{H_d} input, while the corresponding results for m_A, μ input choice are a little less good for m_{H_u} and m_{H_d} , which is attributed to a certain precision loss in our algorithm when passing from one to the other input set, that involves calculations and iterations including two-loop radiative corrections. (This is in particular due to the well-known $Tr[YM^2]$ terms present in the RGE[26, 27], which involve a combination of soft scalar terms, including $m_{H_u}^2$ and $m_{H_d}^2$: this combination vanishes by definition in mSUGRA, and remains zero at all scales in a top-down RG evolution. However, when using bottom-up RGE the approximate $m_{H_u}^2, m_{H_d}^2$ values as obtained from m_A, μ from EWSB conditions Eqs. (32) does not satisfy $Tr[YM^2] = 0$ exactly, and this induces a not completely negligible departure when evolving from low to GUT scales.)

Next, the fourth and subsequent columns give the deviations in the output parameter values corresponding to $\pm 1\%$ deviations of some relevant parameters input values: $M_3, m_{H_u}, m_{Q_{3L}}$, that we chose on purpose as they give the most important sensitivity in other parameters deviations. One can see that the deviations induced to other parameters remain generally reasonable, at the percent level, notably for the gaugino masses and most of the squark and sleptons (except for the one parameter that is varied in each case). In contrast, the deviations induced on the scalar mass term m_{H_u} can be huge even for a moderate percent deviation, i.e. there is a large amplification or dispersion of error which is of course explained from the detailed RGE dependence of m_{H_u} on other soft terms, resulting in a very strong sensitivity on certain other parameters. The same is true to some extent for m_{t_R} . The strong sensitivity of m_{H_u} e.g. on the top mass value and other parameters through its RGE is a well-know feature, but more precisely our illustration here indicate that it will be very difficult to have a precise determination of m_{H_u} at a high GUT scale, even in the very optimistic case where all other MSSM parameters would be know quite precisely. Consequently it will be very difficult to check for eventual universality of the soft scalar mass terms with the squark and slepton soft terms. One can however turn this argument around, and deduce from this illustration that while m_{H_u} plays a crucial role in the (radiative) electroweak symmetry breaking, the sparticle masses at low scale determining most of the collider phenomenology are not very much dependent on its precise value at GUT scale. (This is somewhat similar here to the “focus point” properties observed for large m_0 values in other mSUGRA parameter choices). More generally many features as illustrated in Table 9 may be important to keep in mind for any realistic bottom-up procedure. The above bottom-up RGE procedure had been used in several stages of our analysis, as indicated in the main text.

Table 9: Bottom-up RG evolution of SPS1a parameters from SuSpect 2.41 with illustration of error propagations. Input parameters (2nd column) were obtained from a standard (top-down) SuSpect run from SPS1a input parameters in Eq. (2) (with $m_{top} = 175$ GeV). The third column gives corresponding output values once evolved back to a GUT scale from a bottom-up SuSpect run with general MSSM option. Fourth and subsequent columns give deviations in the output parameter values corresponding to $\pm 1\%$ deviations of some relevant parameters input values as indicated. (Variation range is given explicitly when non-symmetrical)

par.	input(GeV)	GUT output	$\Delta M_3 = \mp 1\%$	$\Delta m_{H_u} = \mp 1\%$	$\Delta m_{Q_{3L}} = \mp 1\%$
$Q_{EW\,SB}$	465.5	$\simeq 2.47 \cdot 10^{16}$	0.1 %	0.1%	0.1%
M_1	101.5	250.004	negl.	negl.	negl.
M_2	191.6	249.998	” ”	” ”	” ”
M_3	586.6	249.999	± 2.2	” ”	” ”
$m_{H_d}^2$	$(179.9)^2$	$(100.004)^2$	$(100.6)^2 - (99.4)^2$	$(100.7)^2 - (99.2)^2$	$(101.2)^2 - (98.7)^2$
$m_{H_u}^2$	$-(358.1)^2$	$(100.017)^2$	$(132.6)^2 - (48.4)^2$	$(64.9)^2 - (124.4)^2$	$(63.7)^2 - (126.4)^2$
(m_A^{pole}) (μ)	398.8 356.9	353			
m_{e_L}	195.5	100.004	100.2–99.8	100.8–99.2	101.5–98.5
m_{τ_L}	194.7	100.004	100.2–99.8	100.8–99.2	101.5–98.5
m_{e_R}	136	99.998	100–99.9	98.4–101.6	96.8–103.1
m_{τ_R}	133.5	99.998	100–99.9	98.4–101.6	96.8–103.1
$m_{Q_{1L}}$	545.8	100.001	121–72	99.7–100.3	99.1–100.8
$m_{Q_{3L}}$	497	100.005	131–52	94.6–104.6	55.2–130.4
m_{u_R}	527.8	99.997	121–72	101–99	101.8–98.1
m_{t_R}	421.5	100.006	140–14	90.6–107.5	81.9–115.3
m_{d_R}	525.7	99.997	121–72	99.4–100.6	98.7–101.3
m_{b_R}	522.4	99.997	122–72	99.4–100.6	98.5–101.5
$-A_t$	494.5	100.009	111 – –89	” ”	” ”
$-A_b$	795.2	100.002	106 – –94	” ”	” ”
$-A_\tau$	251.7	100.002	100 – –99.9	” ”	” ”
$-A_u$	677.3	100.005	108 – –92	negl.	negl.
$-A_d$	859.4	100.001	105 – –95	” ”	” ”
$-A_e$	253.4	100.002	100 – –99.9	” ”	” ”
$\tan \beta$	9.74				

References

- [1] For reviews on the MSSM, see: H. P. Nilles, Phys. Rept. **110**, 1 (1984); R. Barbieri, Riv. Nuovo Cim. **11N4**, 1 (1988); R. Arnowitt and Pran Nath, Report CTP-TAMU-52-93; M. Drees and S.P. Martin, hep-ph/9504324; J. Bagger, Lectures at TASI-95, hep-ph/9604232;

- S.P. Martin, hep-ph/9709356; S. Dawson, hep-ph/9712464.
- [2] B.C. Allanach, C.G. Lester, M.A. Parker and B.R. Webber, JHEP 0009 (2000) 004.
 - [3] B.K. Gjelsten, D.J. Miller and P. Osland, JHEP 0412 (2004) 003 (hep-ph/0410303).
 - [4] B.K. Gjelsten, D.J. Miller and P. Osland, JHEP 0506 (2005) 015 (hep-ph/0501033).
 - [5] G. Weiglein et al, Phys. Rept. 426 (2006) 47 (hep-ph/0410364).
 - [6] J.A. Aguilar-Saavedra et al, Eur. Phys. J. C46 (2006)43 (hep-ph/0511344).
 - [7] There is a very large amount of literature on this subject. For a very non-exhaustive list of relatively recent works, see e.g.: H. Baer, C. Balazs, A. Belyaev, J.K. Mizukoshi, X. Tata and Y. Wang, JHEP **0207**, 050 (2002), hep-ph/0205325; H. Baer and C. Balazs, JCAP **0305**, 006 (2003), hep-ph/0303114; H. Baer, C. Balazs, A. Belyaev, T. Krupovnickas and X. Tata, JHEP **0306**, 054 (2003) [arXiv:hep-ph/0304303]; U. Chattopadhyay, A. Corsetti and P. Nath, Phys. Rev. **D68**, 035005 (2003) hep-ph/0303201; J.R. Ellis, K.A. Olive, Y. Santoso and V.C. Spanos, Phys. Lett. **B565**, 176 (2003), hep-ph/0303043; M. Battaglia, A. De Roeck, J.R. Ellis, F. Gianotti, K.A. Olive and L. Pape, Eur. Phys. J. **C33**, 273 (2004), hep-ph/0306219; M.E. Gomez, T. Ibrahim, P. Nath and S. Skadhauge, Phys. Rev. **D70**, 035014 (2004); A. Djouadi, M. Drees and J. L. Kneur, JHEP **0603**, 033 (2006) [arXiv:hep-ph/0602001]; U. Chattopadhyay, D. Das, A. Datta and S. Poddar; Phys. Rev. D **76**, 055008 (2007) [arXiv:0705.0921 [hep-ph]].
 - [8] J.R. Ellis, K.A. Olive, Y. Santoso and V. Spanos, Phys.Rev. D 69 (2004) 095004 [arXiv:hep-ph/0310356]; J.R. Ellis, S. Heinemeyer, K.A. Olive and G. Weiglein, JHEP 0502 (2005) 013 [arXiv:hep-ph/0411216]; E.A. Baltz and P. Gondolo, JHEP 0410 (2004) 052 [arXiv:hep-ph/0407039]; B.C. Allanach and C.G. Lester, Phys. Rev. D73 (2006) 015013 [arXiv:hep-ph/0507283]; B.C. Allanach, Phys.Lett. B635 (2006) 123 [arXiv:hep-ph/0601089]; R. Ruiz de Austri, R. Trotta and L. Roszkowski, JHEP 0605 (2006) 002 [arXiv:hep-ph/0602028]; E. Baltz, M. Battaglia, M. Peskin and T. Wizansky Phys.Rev. D74 (2006) 103521, [arXiv:hep-ph/0602187].
 - [9] A.H. Chamseddine, R. Arnowitt and P. Nath, Phys. Rev. Lett. 49 (1982) 970; R. Barbieri, S. Ferrara and C.A Savoy, Phys. Lett. B119 (1982) 343; L. Hall, J. Lykken and S. Weinberg, Phys. Rev. D27 (1983) 2359; E. Cremmer, P. Fayet and L. Girardello, Phys. Lett. B **122**, 41 (1983); N. Ohta, Prog. Theor. Phys. **70**, 542 (1983).
 - [10] Review of Particle Physics, Particle Data Group, J. of Phys. G 33 (2006) 1.
 - [11] F. James, M. Roos, Comp. Phys. Commun. 10 (1975) 343.
 - [12] T. Sjostrand, S. Mrenna and P. Skands, JHEP **0605**, 026 (2006) [arXiv:hep-ph/0603175]; T. Sjostrand, L. Lonnblad and S. Mrenna, "PYTHIA", hep-ph/0108264.

- [13] G. Corcella et al, “HERWIG 6”, JHEP 0101 (2001) 010.
- [14] A. Pukhov et al, “CompHEP” [hep-ph/9908288].
- [15] R. Lafaye, T. Plehn and D. Zerwas, hep-ph/0404282; M. Rauch, R. Lafaye, T. Plehn and D. Zerwas, arXiv:0710.2822.
- [16] P. Bechtle, K. Desch and P. Wienemman, Comput. Phys. Commun. 174 (2006)47 (hep-ph/0412012) P. Bechtle, K. Desch, W. Porod and P. Wienemann, Eur.Phys.J.C46:533-544,2006 [hep-ph/0511006]
- [17] R. Lafaye, T. Plehn, M. Rauch and D. Zerwas, Eur.Phys.J. C54(2008) 617 (arXiv:0709.3985 [hep-ph]).
- [18] N. Metropolis, A.W. Rosenbluth, M.N. Teller and E. Teller, J. of Chem. Phys. 21 (1953) 1087; W.K Hastings, Biometrika 57 (1970).
- [19] J.-L. Kneur and G. Moultaka, Phys. Rev. D59 (1999) 015005; J.-L. Kneur and G. Moultaka, ibid, Phys. Rev. D 61 (2000) 095003.
- [20] S.Y Choi, A. Djouadi, M. Guchait, J. Kalinowski, H.S. Song and P.M Zerwas, Eur.Phys.J.C14 (2000) 535 (hep-ph/0002033); S.Y. Choi, J. Kalinowski, G. Moorgat-Pick and P.M Zerwas, Eur. Phys. J. C22 (2001) 563; Addendum-ibid. C23 (2002) 769; ibid hep-ph/0202039; G. Moortgat-Pick et al, Phys.Rept.460 (2008) 131; [arXiv:hep-ph/0507011].
- [21] G.A. Blair, W. Porod and P.M. Zerwas, Phys. Rev. D63 (2001) 017703; Eur. Phys. J. C27 (2003) 263;
- [22] G.A. Blair et al, Acta Phys.Polon. B36 (2005) 3445 [arXiv:hep-ph/0512084].
- [23] See for instance G.L. Kane, TASI lectures, hep-ph/0202185.
- [24] N. Arkani-Hamed, G.L. Kane, J. Thaler and L.-T. Wang, JHEP 0608 (2006) 070 [hep-ph/0512190]; C.F. Berger, J. Gainer, J.L. Hewett, B. Lillie and T.G. Rizzo, arXiv:0712.2965 [hep-ph]; ibid, arXiv:0711.1374 [hep-ph];
- [25] B.C. Allanach, K. Cranmer, C.G. Lester and A.M. Weber, JHEP 0708:023,2007 [arXiv:0705.0487 [hep-ph]].
- [26] K. Inoue, A. Kakuto, H. Komatsu and S. Takeshita, Prog. Theor. Phys. 68, 927 (1982); Erratum: ibid. 70, 330 (1983); ibid. 71, 413 (1984); M. Machacek and M.T. Vaughn, Nucl. Phys. B222 (1983) 83; ibid. B236 (1984) 221; ibid B249 (1985) 70; I. Jack, Phys. Lett. B147 (1984) 405; V. Barger, M.S. Berger and P. Ohmann, Phys. Rev. D47 (1993) 1093; D.J. Castaño, E.J. Piard and P. Ramond, Phys. Rev. D49 (1994) 4882; W. de Boer, R. Ehret and D.I. Kazakov, Z. Phys. C67 (1994) 647; Y. Yamada, Phys. Rev. D50 (1994) 3537; I. Jack and D.R.T. Jones, Phys. Lett. B333 (1994) 372.

- [27] S.P. Martin and M.T. Vaughn, Phys. Rev. D50 (1994) 2282.
- [28] H. Baer, F.E. Paige, S.D. Protopopescu and X. Tata, “ISAJET”, hep-ph/0001086; hep-ph/0312045.
- [29] B.C. Allanach, “SOFTSUSY”, Comput. Phys. Commun. 143 (2002) 305.
- [30] W. Porod, “SPHENO”, Comput. Phys. Commun. 153 (2003) 275.
- [31] A. Djouadi, J-L. Kneur and G. Moultaka, “SuSpect”, Comput. Phys. Commun. 176 (2007) 426 [hep-ph/0211331].
NB the code can be downloaded at: www.lpta.univ-montp2.fr/~kneur/Suspect.html
- [32] ATLAS detector and physics performance Technical Design Report, CERN-LHCC-99-14/15 (1999).
- [33] CMS physics : Technical Design Report v.2 : Physics performance CERN-LHCC-2006-021 (2006), J. Phys. G **34**, 995 (2007).
- [34] B.C. Allanach et al., Eur. Phys. J. C25 (2002) 113 [hep-ph/0202233];
- [35] M.M. Nojiri, G. Polesello and D. R. Tovey, arXiv:0712.2718v2 [hep-ph].
- [36] H-C Cheng, D. Engelhardt, J. F. Gunion, Z. Han and B. McElrath, arXiv:0802.4290 [hep-ph].
- [37] See e.g. U. Heintz, arXiv:0806.1202.
- [38] D. M. Pierce, J. A. Bagger, K. T. Matchev and R. J. Zhang, Nucl. Phys. B491 (1997) 3 [hep-ph/9606211].
- [39] S. Heinemeyer, W. Hollik and G. Weiglein, Phys.Lett. B455 (1999) 179 [hep-ph/9903404]; ibid, hep-ph/0002213.
- [40] For more complete references on Higgs mass radiative corrections, higher order uncertainties etc, see e.g. the review by S. Heinemeyer, Eur. Phys. Jour. C22 (2001) 521 [hep-ph/0108059].
- [41] J.-L. Kneur, R. Lafaye, T. Plehn, M. Rauch and D. Zerwas, in preparation.
- [42] A. Bottino, N. Fornengo, G. Polesello and S. Scopel, arXiv:0801.3334[hep-ph].
- [43] L. Randall and R. Sundrum, Nucl. Phys. B557 (1999) 79; G. Giudice, M. Luty, H. Murayama and R. Rattazzi, JHEP 9812 (1998) 027.
- [44] For a general review e.g.: G.F. Giudice and R. Rattazzi, Phys. Rept. 322 (1999) 419.
- [45] The ALEPH, DELPHI, L3 and OPAL Collab., Phys. Lett. **B565**, 61 (2003), hep-ex/0306033.

- [46] For a summary of sparticle search limits from LEP see <http://lepsusy.web.cern.ch/lepsusy/>
- [47] B.C. Allanach, A. Djouadi, J.-L. Kneur, W. Porod and P. Slavich, JHEP 0409 (2004) 044 [hep-ph/0406166].
- [48] G. Gamberini, G. Ridolfi and F. Zwirner, Nucl. Phys. B331, 331 (1990); B. de Carlos and J.A. Casas, Phys. Lett. B309, 320 (1993).
- [49] R. Arnowitt and P. Nath, Phys. Rev. D46, 3981 (1992); V. Barger, M.S. Berger and P. Ohmann, Phys. Rev. D49, 4908 (1994); P.H. Chankowski, S. Pokorski and J. Rosiek, Nucl. Phys. B423 (1994) 437.
- [50] See e.g. H. Haber, R. Hempfling and A. H. Hoang, Z.Phys. C75 (1997) 539 [arXiv:hep-ph/9609331].
- [51] A. Brignole, G. Degrassi, P. Slavich and F. Zwirner, Nucl. Phys. B631 (2002) 195 [hep-ph/0112177]; Nucl. Phys. B643 (2002) 79 [hep-ph/0206101].
- [52] P. Skands *et al.*, JHEP 0407 (2004) 036; P. Skands *et al.*, arXiv:0801.0045 [hep-ph].